

Smart nano-architectures as potential sensing tools for detecting heavy metal ions in aqueous matrices

Tahir Rasheed^{a*}, Sameera Shafi^b, Farooq Sher^c

^a*Interdisciplinary Research Center for Advanced Materials, King Fahd University of Petroleum and Minerals (KFUPM), Dhahran 31261, Saudi Arabia.*

^b*Institute of Chemistry, The Islamia University of Bahawalpur, Bahawalnagar campus 62300, Pakistan*

^c*Department of Engineering, School of Science and Technology, Nottingham Trent University, Nottingham NG11 8NS, UK*

*Corresponding author: Email address: tahir.rasheed@kfupm.edu.sa (T. Rasheed).

Abstract

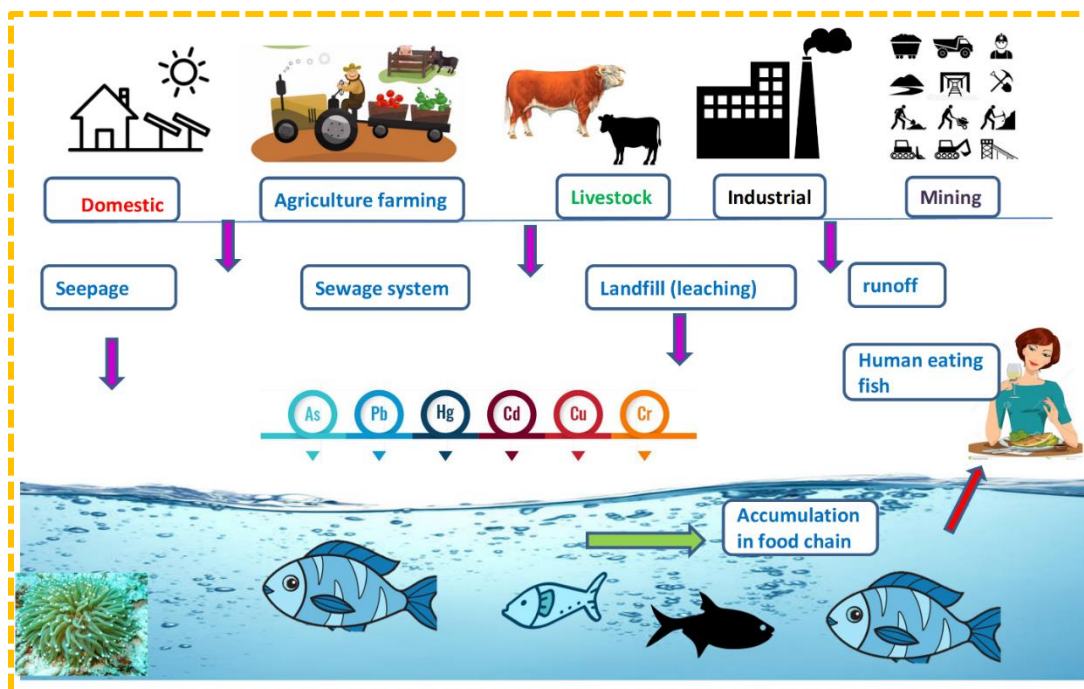
The discharge of heavy metal ions into water resources as a result of human activities has become a global issue. Contamination with heavy metal ions poses a major threat to the environment and human health. Therefore, there is a dire need to probe the presence of heavy metal ions in a more selective, facile, quick, cost-effective and sensitive way. Conventional sensors are being utilized to sense heavy metal ions; however, various challenges and limitations like interference, overlapping of oxidation potential, selectivity and sensitivity are associated with them that limit their in-field applicability. Hence, nanomaterial based chemical sensors have emerged as an alternative substitute and are extensively employed for the detection of heavy metal ions as a potent analytical tool. The incorporation of nanomaterials in sensors increases their sensitivity, selectivity, portability, on-site detection capability and device performance. Nanomaterial based electrodes exhibit enhanced performance because surface of electrode at nano-scale level offers high catalytic potential, large active surface area and high conductivity. Therefore, this review addresses the recent progress on chemical sensors based on different nanomaterials such as carbon

29 nanotubes (CNTs), metal nanoparticles, graphene, carbon quantum dots and nanocomposites for
30 sensing heavy metals ions using different sensing approaches. Furthermore, various types of
31 optical sensors such as fluorescence, luminescence and colorimetry sensors have been presented
32 in detail.

33 **Keywords:** Pollution; Smart nanomaterials; Heavy metal ions; Optical chemical sensors;
34 Nanosensors and Aqueous matrices.

35 **1. Introduction**

36 Industrial, agriculture and domestic sectors are primary sources to discharge heavy metal ions in
37 the eco-system. Some of the heavy metal ions like Zn^{2+} , Mn^{2+} , Fe^{2+} and Cu^{2+} are required by living
38 organisms in trace amounts to carry the fundamental processes like metabolism, growth and
39 development of different organs. While some of these heavy metal ions including Cd^{2+} , As^{3+} , Hg^{2+}
40 and Pb^{2+} are considered toxic substances and contaminants even at very low concentrations that
41 can be termed as a serious risk to the environment and human health [1-6]. Additionally, there are
42 some natural sources such as erosion of soil and rock, rainwater and weathering from where heavy
43 metals are also added to the environment [7]. On the other hand, leaching of metals from different
44 sources like waste dumps, runoffs, livestock manures and roadwork are some of the other sources
45 (secondary sources) of heavy metal pollution. Fig. 1 illustrates the primary and secondary sources
46 of heavy metal pollution in the eco-system. Heavy metals occur in the form of ions, elements or
47 complexes and are non-degradable.



48

49

Fig. 1. Different sources of heavy metal pollution in the ecosystem.

50 Furthermore, heavy metals are elements with an atomic number of more than 20 and having a
 51 density of higher than 5 g/cm^3 . They originally belong to metalloids, transition elements and post-
 52 transition elements [8, 9]. Their accumulation (even at a minute level) in the body causes severe
 53 health risks and most of them are carcinogenic [4, 10-17]. Maximum concentration limits and
 54 linked health risks related to heavy metals have already been reported in the literature [7]. The
 55 non-biodegradability, dissolution in water, ability to form aggregates in various parts of the body
 56 and delayed half-life makes these species more lethal to human life [18]. The mechanism of their
 57 toxicity involves their interaction with the cell proteins and DNA. This interaction leads to the
 58 change in protein conformation that in turn results in carcinogenesis. The other detrimental effects
 59 of heavy metal ions pollution on human life are lung damage, vomiting, nausea, high blood
 60 pressure, fatigue, hepatotoxicity, nephrotoxicity, neurotoxicity, headache and depression are the
 61 main causes of heavy metal ions toxicity (Fig. 2) [19].

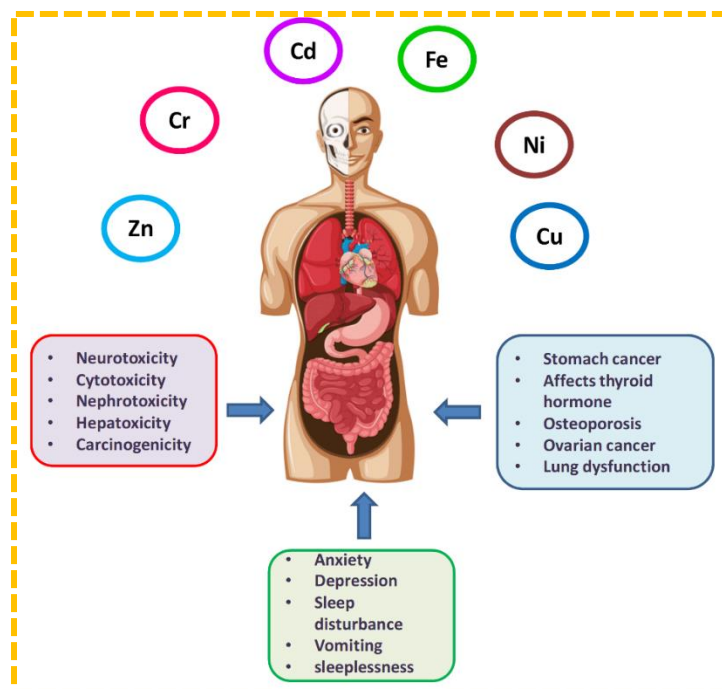


Fig. 2. Hazardous effects of heavy metals on human health.

62

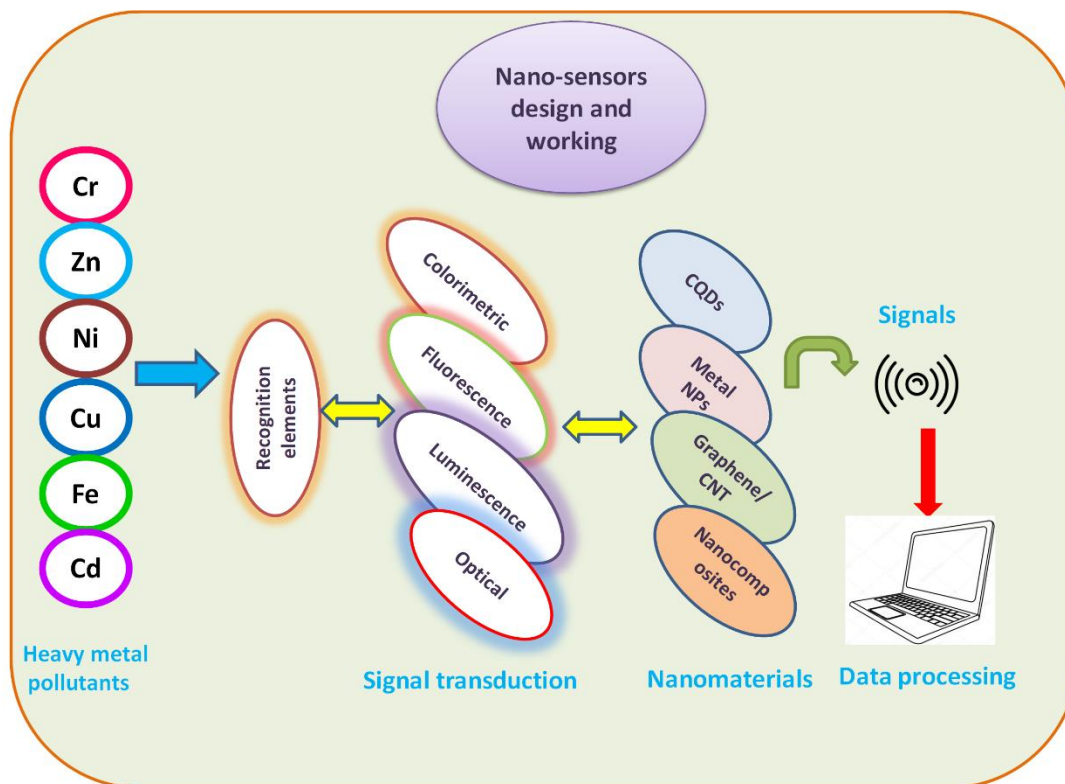
63

64 Therefore, the accurate detection and determination of these toxicants is a pressing issue in recent
 65 years [20]. Some of the traditionally employed analytical techniques for the detection and
 66 determination of these metal ions include microprobes, X-ray fluorescence spectroscopy, capillary
 67 electrophoresis, ion chromatography, ultraviolet-visible spectroscopy, inductively coupled
 68 plasma-mass spectroscopy, atomic emission spectroscopy and atomic absorption spectroscopy
 69 [21-23]. These analytical techniques are selective and very sensitive however because of some
 70 limitations associated such as (1) High operating expenditures, (2) limits of hiring skilled
 71 individuals, (3) expensive and time intensive, (4) complex operating procedures (5) difficult
 72 sample preparation and (6) hard for real-time evaluation, limit their in-field applications [20].

73 This necessitates the development of a new technique that can detect these toxic metal ions with
 74 greater simplicity and accuracy. In this regard, chemical sensing has emerged as a promising
 75 modality for the accurate and on-site identification of these metal ions. Among a variety of
 76 chemical sensors, nanomaterial-based sensors are promising candidates for the purpose. The

77 emergence of nanomaterial-based sensors owes to their distinctive features such as great
78 adsorption power, higher surface reactivity, higher catalytic efficiency and larger surface area [24-
79 28].

80 A nanosensor consists of three components: (1) nanomaterial, (2) recognition element and (3)
81 signal transducer. Several nanomaterials such as silicon materials, carbon-based materials and
82 metallic nanoparticles (NPs) have been utilized widely to design a nanosensor. Fig. 3 portrays the
83 design and working mechanism of various nanosensors. Nanosensors can be designed to sense a
84 single analyte known as single plex or multiple analytes called multiplex. The higher degree of
85 functionalization, the higher surface to volume ratio and higher reactivity enhance the nanosensor's
86 sensitivity [29]. Furthermore, the formation of nanocomposites, organic-ligand attachment and
87 covalent functionalization play a vital role to improve the selectivity and sensitivity in the
88 identification of heavy metal ions. The reproducibility and lower limit of detection (LOD) are the
89 other important parameters possessed by the nanomaterial-based sensors [22].



90

91 **Fig. 3.** Schematic illustration of design and working principle of various nanosensors for sensing

92 metal ions.

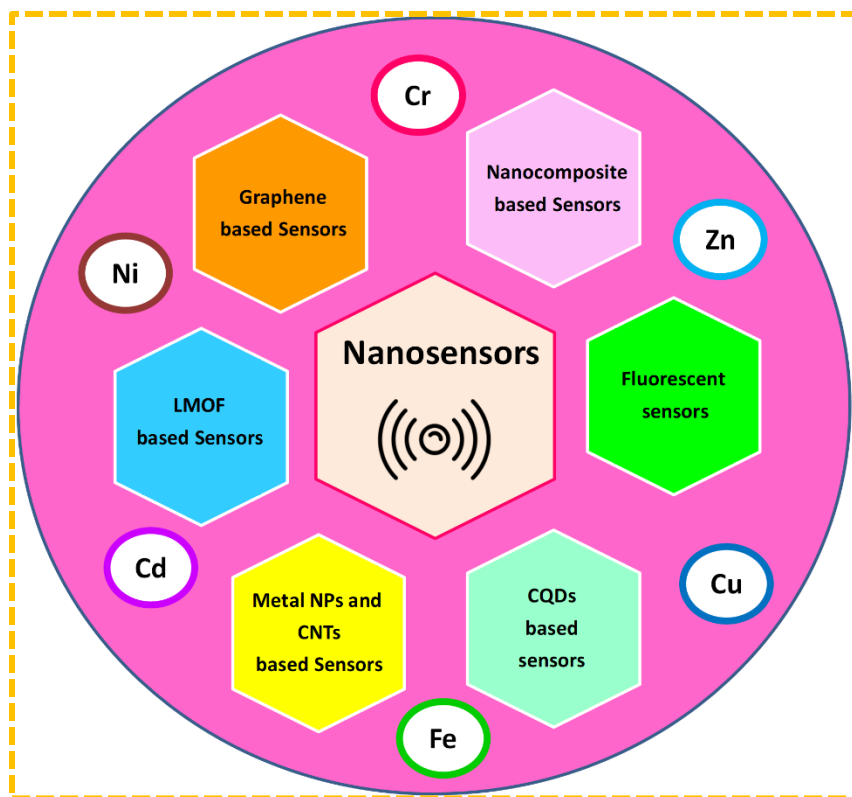
93 This review emphasizes the modern advancement in the area of optical chemical sensors based on

94 different nanomaterials. Furthermore, the designs, working and sensing mechanisms of

95 nanosensors for the detection of heavy metal ions have been discussed in detail. Finally, the

96 conclusion and future recommendations have been presented. Fig. 4 represents different types of

97 nanosensors that are discussed in the present study.



98

99

100 **Fig. 4.** Various types of nanomaterial-based nanosensors for the detection of heavy metal ions.

101 **2. Optical sensors**

102 Optical chemical sensors (OCSs) are widely employed for on-site identification of heavy metal
 103 ions. The transduction element of OCSs absorbs electromagnetic radiations for producing signals.

104 The specific optical factors get changed by the interaction of radiation with the test sample that
 105 could be related to analyte quantity in the sample. Optical chemical sensors worked on the principle

106 of variation of optical characteristics (lifetime, emission, transmission and absorption) because of

107 the linkage of organic dye (immobilized indicator) with analyte [30, 31]. Target-induced-

108 aggregation/anti-aggregation and surface alterations of nanomaterials may change the optical

109 characteristics of nanomaterials chemical sensors based on the nanomaterial. In addition, the

110 framework is dependent upon the suitable choice of solid matrix, with appropriate morphology,

111 functionalization and immobilization strategies for these constituents [32]. Fluorescent, surface
112 plasmon resonance (SPR) sensors, surface enhanced Raman scattering (SERS) optical sensors,
113 fluorescence and luminescence sensors have also been demonstrated in this review. Special focus
114 is given to utilization of nanomaterials in the development of these sensors.

115 **2.1. Fluorescent sensors**

116 Fluorescence based nanosensors consist of the fluorescent element that signals receptor component
117 and binding site to bind the particular analyte [11-14, 33-35]. Quantum dots (QDs) have been
118 extensively employed as an alternative to the dyes-based fluorophore. The unique optical
119 characteristics such as high stability towards photo bleaching, narrow emission, great quantum
120 yield and wide range of absorption spectra as well as excellent H₂O solubility, great photo-stability
121 and changeable quantum size in a broad emission range make QDs promising alternatives for
122 sensing and biosensing of a variety of analytes [36, 37]. Because of broad excitation profiles,
123 multiplexed detection potential, higher quantum efficiencies, size dependent fluorescence
124 emission peaks, great photostability and narrow emission spectra the quantum dots are
125 advantageous to employ as fluorophores [38]. The structures of graphene QDs (GQDs) and carbon
126 dots (CDs) are free from heavy metals.

127 Moreover, these contain extraordinary surface functionality and very good biocompatibility that
128 makes them very effective candidates for the fluorescent identification of metals [39, 40]. Selective
129 linkage sites are formed on the sensor surface that is permitted by molecular imprinting that assists
130 particular linkage of analytes. The facile synthesis and stability are major advantages of formed
131 sensing materials. Based upon the ion-imprinted dual emission quantum dots nanohybrids
132 (CdTe@SiO₂@CdSe) the ratiometric-fluorescent probe has been developed for the identification
133 of Cd²⁺ ions in aqueous samples [41]. Probe structure was found based on covalently bonding

134 green emitting CdSe QDs at the surface of silica nanoparticles that was surrounded by red emitting
135 CdTe QDs. By chemical etching with ethylene-diamine tetra-acetic acid, the particular Cd²⁺ ions
136 detection sites upon the surface were formed that extinguished the fluorescence (green) of CdSe
137 quantum dots on nanosensor's external side. By exposing nanohybrid to various quantities of Cd²⁺
138 ions, the green fluorescence is progressively reinstated and internal red fluorescence remains the
139 same. As a result, the identifiable fluorescence of different colors was perceived when it is in
140 contact with Cd²⁺ ions. The ratiometric sensor showed very good sensitivity at optimized
141 conditions with LOD of 25 nM. Another study, reports the development of unique luminescence
142 solid state material (QD-LDH) for on-site concurrent identification of Hg²⁺, Cd³⁺ and Pb²⁺ ions in
143 H₂O [42]. The architecture of the nanosensor is based on layered double hydroxides (LDH) and
144 manganese-doped ZnS QDs capped with the glutathione (GSH-Mn-ZnS QDs). The LDH function
145 inhibits the accumulation of quantum dots (QDs) in solid nanocomposite and improved
146 luminescence in aqueous solution as compared to the dispersed quantum dots. Moreover, the
147 chemical and thermal stability of quantum dots is also strengthened by LDH containing
148 nanocomposite. A turn-off response was observed by the introduction of Hg²⁺, Cd³⁺ and Pb²⁺ ions.
149 The luminescence intensity of nanosensor disappeared as the nanosensors come in contact with
150 analytes. Remarkable sensitivity and selectivity were portrayed by the sensor with LOD of 0.93
151 μM for mixed metal ions. Likewise, the identification of Hg²⁺ ions in raw-water and tape water
152 samples was carried out with the help of nitrogen-doped-carbon based nanosensor QDs (N-CQDs)
153 that was hydrothermally synthesized as a fluorescent probe [43]. The formation of sensor utilized
154 folic acid (carbon and nitrogen source). For label-free identification of Hg²⁺ ions the prepared N-
155 CQDs (size approximately 4.5 nm) assisted as a sensitive sensor. Noteworthy quenching of
156 fluorescence intensity is driven by the introduction of Hg²⁺ ions that lead to non-radiative electron

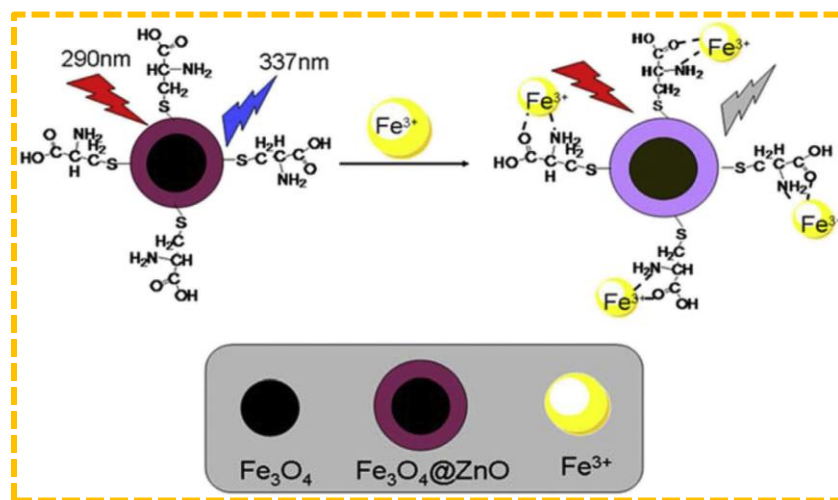
157 shift from the high energy states to Hg^{2+} ions d-orbital. The N-CQDs have shown specificity for
158 Hg^{2+} ions within the existence of a great quantity of other various competitive metal ions and can
159 be termed as “turn-off” fluorescent sensors. The LOD was calculated as low as 0.23 mM. In
160 another documented report, the Gold nano-clusters based CdTe quantum dots were developed. The
161 prepared nanocomposite material showed high selectivity and sensitivity towards fluoride and
162 Hg^{2+} ions. This nanosensor was developed from a bovine-serum-albumin protein-conjugated Au
163 nanocluster and from tripeptide-capped CdTe quantum dots [44]. The salt-initiated
164 conglomeration upon introduction of Hg^{2+} ions driven to critical reduction approximately up to
165 74% of nanosensor photoluminescence. The LOD towards Hg^{2+} and fluoride ions was determined
166 as 9 and 117 nM respectively.

167 Graphene oxide (GO) is another useful nanomaterial that is non-toxic and contains a carboxylic
168 acid group that could be utilized to conjugate the various biomolecules and deoxy-ribonucleic acid
169 functionalized with amine by a covalent bond. Further, GO is an economical fluorescence radiation
170 quencher (acceptor) that may be easily formed on large scale. The fluorescent features of GO can
171 easily be tuned by modifying the surface functionalities. Therefore, graphene oxide obtained great
172 consideration in sensing heavy metals [45]. Ju and his colleagues [39] revealed a simple technique
173 to synthesize the greatly fluorescent nitrogen-doped GQDs (N-GQDs) for the identification of Fe^{3+}
174 ions. GQDs are treated hydrothermally with hydrazine for the preparation of N-GQDs as a sensing
175 platform. The presence of oxygen based functional motifs in N-GQDs showed improved
176 fluorescence potential with the blue-shifted-energy that may be due to the existence of nitrogen
177 (electron withdrawing nature) in the structure of nanosensor. The PL intensity of N-GQDs has
178 been reduced by the incorporation of Fe^{3+} ions. This reduction in PL owes to the chelation of Fe^{3+}
179 ions with nitrogen (N) of N-GQDs. In real water samples, the LOD of 90 nM was determined by

180 the job's plot method. Through the electrolysis of graphite, the sulfur-doped-GQDs (S-GQDs)
181 synthesis has been reported [40]. The S-GQDs showed a more sensitive response to Fe^{3+} ions in
182 comparison to B-GQDs, GQDs and NGQDs. Noteworthy, reduced fluorescence intensity for
183 SGQDs was noticed at 0.7 mM for Fe^{3+} ions concentration on the other hand the fluorescence of
184 B-GQDs, GQDs and NGQDs remains unaltered. Greater sensitivity in human serum (with LOD
185 of 4.2 nM) was displayed by a probe. For the identification and recognition of Fe^{3+} ions atoms in
186 H_2O , the greatly selective and sensitive graphitic CQDs (GCQDs) were developed through
187 electrochemical ablation of graphite electrodes [46]. The solubility of the probe in water was
188 improved by oxygen containing functional moieties (-COOH and -OH). Moreover, because of the
189 development of complexes between phenolic -OH moieties of GCQDs and Fe^{3+} ions the probe
190 showed greater sensitivity (LOD of 2 nM). By exfoliation of graphene oxide into the graphene
191 oxide (GO) sheets through ultra-sonication in aqueous media, the GQDs based developing zero-
192 D-materials synthesized within a range of 3 to 20 nm. In conjunction with the best surface grafting
193 feature, the material also contained carrier transport portability, great surface range and
194 predominant chemical and thermal steadiness. Ran and his co-workers [47] utilized GQDs and
195 silver-based nanoparticles embodied GQDs (AgNPs/ GQDs) for recognition of Ag^+ ions and bio-
196 thiol molecules as glutathione (GSH), cysteine (Cys) and homocysteine (Hcy). The FL intensity
197 of novel fluorescent material GQDs was decreased after incorporation of Ag^+ ions. The reduced
198 fluorescence that was dosage-dependent owes to the synthesis of AgNPs/GQDs hybrids. In
199 addition, when bio-thiols were introduced into the solution, the fluorescence of GQDs was
200 diminished and it has been accredited to Ag-S bond formation. The probe demonstrated ultra-
201 sensitivity with LOD of 3.5 and 6.2 nM for Ag^+ ions and Cys respectively. Lu and coworkers [48]
202 exhibited single-step sulfur and oxygen co-doped graphitic carbon nitride QDs (OS-GCNQDs)

203 synthesis through a reaction between thiourea and citric acid in warming conditions. The
204 synthesized OS-GCNQDs showed great quantum yield (14.5%) and demonstrated variable
205 fluorescence responses in the existence of various metal ions in similar conditions. The PL
206 intensity of OS-GCNQDs has been quenched through the incorporation of the Hg^{2+} ions that could
207 be because of great affinity of thiourea moieties and amino functional moieties existing on the
208 surface of nanocomposite with Hg^{2+} ions. The OS-GCNQDs ascertained greatly sensitive that was
209 capable of selectively towards Hg^{2+} ions with LOD of 0.37 nM. Similarly, other documented
210 reports also investigated the detection of heavy metal ions in aqueous media through graphene and
211 graphene oxide-based optical sensors [48, 49]. The addition of graphene oxide or graphene in the
212 nanosensors potentially enhanced the sensitivity in heavy metal detection. For sensing heavy
213 metal ions, metal-based nanomaterials have been widely employed because of their great
214 biocompatibility, easy fabrication, plasmonic features and optical characteristics [28, 50, 51].
215 To enhance the detection of heavy metals, metallic nano-structures consisting of aluminum, silver
216 and gold plasmonic NPs have been broadly utilized [52]. For spectral sensing of heavy metals,
217 one-step preparation of CuS, NiS & ZnSNPs, CuSNPs and NiS NPs has been reported [53]. By
218 utilizing tri-sodium citrate and sodium sulfide, the prepared nanoparticles were stabilized in
219 aqueous media. For spectral detection of Pb^{2+} , Cd^{2+} and Hg^{2+} ions at very low concentrations, the
220 solid nanoparticles were being utilized as optical sensors. In the existence of ions of heavy metal,
221 absorption potentials of nanoparticles have enhanced and this was connected to basic accumulation
222 of NPs or variations within the nearby atmosphere of the nano substances that produced variations
223 within characteristic surface-plasmon-resonance. For Hg^{2+} ions identification, NiS NPs were found
224 beneficial while CuS NPs and ZnS NPs were found capable to identify Hg^{2+} , Cd^{2+} and Pb^{2+} ions
225 with LOD of 0.1-1 mM and 0.1-1.5 mM, respectively. Li and his colleagues [54] demonstrated the

226 fluorescent nanoprobe based upon L-cysteine (L-Cys) capped $\text{Fe}_3\text{O}_4@ZnO$ ($\text{Fe}_3\text{O}_4@ZnO@L$ -
 227 Cys) for profoundly specific Fe^{3+} ions identification. Upon the addition of Fe^{3+} ions solution,
 228 nanosensor fluorescent potential was quenched. This was connected to the interaction of Fe^{3+} ions
 229 with L-Cys. With LOD of 3 nM/L, over a series of competing ions such as Co^{2+} , Mn^{2+} , Cu^{2+} , Cd^{2+} ,
 230 Mg^{2+} , Al^{3+} and Pb^{2+} ions the nanoprobe showed high selectivity in identifying Fe^{3+} ions in serum
 231 and wastewater (Fig. 5).



232
 233 **Fig. 5.** The binding mechanism of $\text{Fe}_3\text{O}_4@ZnO@L\text{-Cys}$ with Fe^{3+} [54]. Licensed under a Creative
 234 Commons Attribution 4.0 International License.

235
 236 Shahat and his coworkers [55] synthesized MSNPs based functional material, wherein organic
 237 ligand, N,N' di (3- carboxysalicylidene)-3,4-diamino-5-hydroxypyrazole (DSDH) was attached to
 238 the mesoporous silica (MS). Through Vander-Waals forces, covalent bonds and hydrogen bonding
 239 the plenteous hydroxyl moieties on MS surface allowed conjugation of DSDH. The obtained
 240 material was employed for Co^{2+} ions identification in aqueous media. The absorbance intensity of
 241 the probe was enhanced by introduction of Co^{2+} . This was credited to the interaction between Co^{2+}
 242 ions with DSDH. With LOD of 0.24 mg/L, the probe demonstrated to be sensitive in recognizing
 243 Co^{2+} ions. The synthesis of conjugate nanomaterials (CNMs) has been accomplished with the

244 ligand (organic), ammonium (4-chloro-2-mercaptophenyl) carbamodithioate (ACMPC) that
245 consist of sulfur donor element by utilizing a coordinate reaction approach by functionalizing
246 MSNPs. In another study, Awual and coworkers [56] documented a ligand conjugated
247 nanomaterial for Hg^{2+} ions identification in an aqueous solution, the resultant sensor was found
248 selective and sensitive toward analyte. As within the case of DSDH, through reversible covalent
249 bonds, Vander Waals force and hydrogen bonding the attachment between SNPs and ACMPC
250 occurs. The color variation from colorless to yellow led to enhance in intensity of absorbance on
251 the addition of Hg^{2+} ions to CNM solution at optimum pH 5.2 and this was observed through
252 ultraviolet-visible spectroscopy. The formation of (ACMPC)- Hg^{2+} complex was credited to the
253 selectivity of CNMs. With LOD of 0.26 mg/L, the nanosensor showed high sensitivity in
254 identifying Hg^{2+} ions. Cao and his coworkers [57] have prepared mono-layer graphite type C_3N_4
255 (g- C_3N_4) as a fluorescence sensor for Ag^+ ions identification in real H_2O . The sensor reached a
256 LOD of 52.3 nmol/L in optimized conditions for the Ag^+ ions without obstructions to the co-
257 existing of miscellaneous metal ions such as Cd^{2+} , Al^{3+} , Ca^{2+} , Ni^{2+} , Co^{2+} , Mg^{2+} , Pb^{2+} , Mn^{2+} , Zn^{2+} ,
258 Hg^{2+} , K^+ , Be^{2+} , Fe^{3+} and Ba^{2+} . Additionally, the obstructions of co-existing Cu^{2+} ions within the
259 sample could be screened by EDTA chelate incorporation. Preparation of nano-aggregates of
260 pyrene polymer as a probe (fluorescent) for identification of Sr^{2+} ions in solution has been reported
261 [58]. With LOD of 9 nM, the fluorescent intensity of the probe quenched upon the addition of Sr^{2+}
262 ions. Over a broad range of competing metals ions such as Pb^{2+} , Hg^{2+} , Cd^{2+} , Zn^{2+} , Ag^+ , Co^{3+} , Cu^{2+} ,
263 Mn^{2+} , Fe^{3+} , Al^{3+} , Ba^{2+} , Mg^{2+} , Ca^{2+} , Cs^+ , K^+ , Li^+ and Na^+ , the nanosensor displayed high selectivity
264 for detection of Sr^{2+} ions. The hydrophobic nature of pyrene moieties permitted them at first step
265 stacked in water that driven to excimer emission. Attachment of the Sr^{2+} ions to host gave

266 alterations in conformation that formed the cavity to fit Sr^{2+} ions by enhancing gap between pyrene
267 (two) motifs. Consequently, the nanosensor fluorescence intensity was quenched.

268 **3. LMOFs implication for detecting Persistent metal ions**

269 Herein, metal ions can be classified into three major categories. The group that is detected in a
270 broader sense using LMOFs essentially Al^{3+} , Hg^{2+} , Fe^{3+} , Cu^{2+} , Cr^{3+} ions, the other group of metal
271 ions comprise Eu^{3+} , Tb^{3+} , Sm^{3+} , Dy^{3+} ions called repetitive metal ions and lanthanide Ln^{3+} metal
272 ions respectively, whereas the third group of metal ions is hardly detected using LMOFs.
273 Moreover, the detection limit, applicable strategies, sensitivity, selectivity, structure signal,
274 mechanism response relationships and parameters like Stern -Volmer constant for each metal ion
275 can conduct an efficient sensing approach with adequate detection considerations.

276 **3.1. Detection of mercury (II)**

277 Facile and faster detection of Hg^{2+} ions for human safety from a catastrophe such as Minamata,
278 whereas LOD is $2 \mu\text{g/L}$ reported by US Environmental Protection Agency. There are varied
279 methodologies implemented for Hg^{2+} ions sensing utilizing LMOFs, for example, 1D constituting
280 MOF-composites [59], ratiometrically 2-dimensional detectors [60], chemo-dosimeter detector
281 comprised of MOF [61], approach for probing 2D-dual solvents [62], (d)-LMOFs [63], 2-
282 dimensional probes [64], lanthanide(+3) ions applied for post-improvement of (d)-LMOFs [65],
283 implications of coordination-polymer-nanoparticles (CPNPs) [66]. There are many fruitful merits
284 and incompetent demerits that have been noticed in every category. After the post-synthetic
285 incorporation of Eu^{3+} ions, $\text{Eu}^{3+}/\text{CDs}@\text{MOF-253}$ composite represents simultaneously both the
286 CDs centered emission (ICD) and characteristic sharp emissions of Eu^{3+} ions originating from the
287 Eu^{3+} ions lowest emitting state. Further, IEu^{3+} showed no considerable variation while 1-
288 dimensional quenching effect was revealed in IQDs by way of enclosed quantum dots (QDs)

289 surface-association of oxygen atoms and Hg^{2+} ions. Consequently, an increment of 7.5 multiple
290 was indicated by $\text{IEu}^{3+}/\text{IQDs}$, in comparison to the primary ratio. Proficient discriminativeness of
291 $\text{Eu}^{3+}/\text{QDs}@\text{MOF-253}$ having 13 nM LOD for Hg^{2+} ions affirmed such effect merely in Hg^{2+} ions,
292 although different metal ions were also available. In addition, Hg^{2+} ions could cause red coloration
293 altered from blue suggesting the above-mentioned composite to perform like colorimetric probe
294 [60]. Remarkable chemical alteration including covalent bond manufacturing and splitting
295 provides the basis for non-reversible conversion of obvious signal accompanying identification of
296 analyte using chemodosimeter sensors.

297 Owing to the existence of bulky butyne groups, rotation of carbonyl group was hindered resulting
298 in FL responsive $\text{UiO-66}@\text{Butyne}$. Through an irreversible oxymercuration reaction, UiO-
299 $66@\text{Butyne}$ exhibits a 1D quenching response to Hg^{2+} ions. The loss of alkyne functionality was
300 shown by a decreased peak at 2950 cm^{-1} in FT-IR spectroscopy after treatment with Hg^{2+} ions. The
301 presence of concentrated sulfide is unfavorable because compounds comprising sulfur and
302 nitrogen atoms experience oxidative cleavages at ambient conditions when preserved for a longer
303 duration, although Hg^{2+} ions have been appropriately diagnosed via LMOFs inhabiting these
304 moieties. These display non-renewable sensitivity in comparison to other probes like fluoro-
305 /chemo-sensors. Fabrication of linking agent-functionalized (d)-LMOFs has been considered a
306 high potential category for sensing Hg^{2+} ions. Nitrogen donor-guest communication parts are a
307 vital constituent of functional ligands [67], sulfur-supported were on the other hand [63] also few
308 residing oxygen units [67]. Scarcely, variation in molecular design or molecular breakage could
309 affect the procedure of identifying Hg^{2+} ions [63]. Detection-limit of 9.9 pM demonstrated higher
310 sensitivity for Hg^{2+} ions by a zinc-based MOF with the representation of $[\{\text{Zn}(4,4'\text{-AP})(5\text{-AIA})$
311 $\}.\text{(DMF)}]_{0.5n}$, and proved with photoluminescent measurements. The introduction of Hg^{2+} ions

312 brought a change in the stretching peak position of carbon and nitrogen bond as shown in FT-IR
313 measurements. Moreover, nitrogen (1s) X-ray photoelectron spectroscopy measurements for
314 [$\{Zn(4,4'-AP)(5-AIA)\} \cdot (DMF)_{0.5n}$] shows a peak at ~ 403.57 eV for coordinated-amino group,
315 ~ 402.36 eV for azo-group and ~ 399.10 eV for pyridine-group, enclosed in a wide peak at ~ 400
316 eV. Interaction of Hg^{2+} ions with [$\{Zn(4,4'-AP)(5-AIA)\} \cdot (DMF)_{0.5n}$] residing nitrogen units
317 resulted in shifting of peaks in the redder zone around ~ 405.53 eV, attributable to Hg^{2+} ions
318 incorporation. The Hg^{2+} ions receive electrons from azo-groups during communication of N_2 group
319 with Hg^{2+} ions as displayed by the practical investigations. Until now, literature explained higher
320 K_{SV} and LOD for responsive and discriminative identification of Hg^{2+} ions adopting particular soft
321 N-constituting impressive architecture of d-LMOFs. Formerly, a small FL shoulder is exhibited at
322 around 410 nm while a bright Photo-luminescent radiance has been noticed at around 350 nm for
323 Cd-EDDA skeleton. The above given explanation corresponds to LLCT and LMCT reactions
324 (processes), accordingly [64]. The use of Cd-EDDA in metal ions sensing reveals that as the Hg^{2+}
325 ions concentration rises that is connected to the LMCT process. The obtained Stern-Volmer
326 constant (KSV) 4.3 mM and identification-limit 10 nM were observed in the presence of 0.21 mM
327 Hg^{2+} ions and 8.2 times improvement with the given ratio. Ligand's reformation and the existence
328 of Hg^{2+} ions were considered the fundamental requirements for Cd-EDDA compound breakage
329 which consequently reduced LMCT and were confirmed with mass-spectroscopy, FT-IR and
330 PXRD. Thus, in the event of rapid simultaneous presence of LLCT and LMCT processes in PL
331 emission of (d)-LMOF, the ratio of ILLCT/ILMCT may be considered as a 2D ratiometric
332 response in the sense that when the framework collapses, the ratio of ILLCT/ILMCT may be
333 considered as a 2D ratiometric response. The ILMCT will drop, while the ILLCT could increase
334 due to ligand–metal ion complexation resulting in an increase in 2D ratiometric ILLCT/ILMCT

335 response. The detection limit of Hg^{2+} ion sensing employing LMOFs has been reported to be in
336 the order of magnitude equal to nM level [64, 68]. Simultaneously, variation in the compound's
337 photo luminescent radiance intensity occurred owing to shifting of electronic cloud from
338 compound to Hg^{2+} ions resulted due to communication of Hg^{2+} ions and functional-ligand,
339 particularly nitrogen donors, residing zinc-LMOF demonstrated ligand rooted radiance while
340 concentrating the connection between mechanism response and structure signal. Although,
341 efficient fabrication of potential Zn^{2+} -LMOFs due to its dissolution in H_2O and photo-durability
342 of the structure are demanded while reproducibility of Zn^{2+} -LMOFs depend on specified
343 functional ligands. The LOD up to level of pM were noticed for gold nanocomposites@UiO-66
344 [69] and DSM@7 [70], built on MOF. In addition, KSV value for Eu^{3+} @post-improved UiO-66
345 approached to μM level. Appropriate incorporation of enclosed guest compounds inside porous
346 MOF, employs MOF-supported composite to recognize Hg^{2+} ions proficiently nonetheless,
347 percolation of such kind of sensors must be thoroughly analyzed for practical implications.

348 **3.2. Detection of Al^{3+} ions**

349 Al^{3+} ions in high amount not only affects the well-being of humans but also can cause serious
350 damage to the human body since it is not a scarce constituent essential for humans. This is a
351 reduction in the haste with which Al^{3+} ions are detected. Many efforts have been made to detect
352 Al^{3+} ions using LMOFs and several methodologies have been used in this line. The sensors
353 extinguishing framework of emissive LMOFs resulting in host-signal alteration in response
354 generation and signal transduction are termed as sacrificial sensors. The bonding of organic-ligand
355 and Al^{3+} ions supports various redundant reaction procedures. Intending to recognize Al^{3+} ions,
356 Singha et al. [71] applied 3,5-diamino-1,2,4-triazole (DATZ) and 4,4'-oxybis(benzoic acid)
357 (H_2OBA) to synthesize $[\text{Co}(\text{OBA})(\text{DATZ})_{0.5}(\text{H}_2\text{O})]$, a triazole-supported (d)-LMOF. Aromatic

358 ligands attached with metal ions underwent intra-ligand π^* -n and π^* - π^* electronic transitions
359 instigating λ_{\max} around 407 nm while the excitation wavelength was 283 nm. In comparison to
360 preliminary emission, translocation of λ_{\max} approximately 24 nm with a signal intensification
361 multiple of 6.3 was noticed when [Co (OBA) (DATZ)_{0.5}(H₂O)] ((d)-LMOF) was implemented for
362 ion identification, however, displayed insignificant variation in the presence of contrasting metal
363 ions. The attachment of free N-atoms constituent of triazole-ligand (-NH-) and Al³⁺ ions supplied
364 a source for signal-transduction discriminatively. Other metal ions interact with free amine groups
365 via Lewis acid-base interactions, whereas Al³⁺ ions can subtract an H⁺ from the NH group of the
366 triazole ring and create triazolate with the amine groups (NH₂) acting as Lewis basic sites due to
367 their high charge-to-size ratio. The blue shift in PL emission peak of frameworks is caused by
368 electrostatic interaction between Al³⁺ ions and the triazolate ring. Furthermore, triazolate
369 production enhances the overall electron density on DATZ, resulting in turn-on luminescence
370 behavior. Because of the limited possibility of forming a triazolate ring in acidic conditions, the
371 results reveal a 2.8 times enhancement that is approximately 3 times less than the value obtained
372 in the initial pure aqueous medium. Based on the strength of architectural uniqueness, revocable
373 pathway and discriminative identification of Al³⁺ ions, it was recommended as an excellent
374 instance of chemical communication betwixt compound and metal ions. Additionally, the
375 maximum LOD was found to be remarkably at high-level in comparison with [Co (OBA)
376 (DATZ)_{0.5}(H₂O)] that was observed with a detection limit of 57.6 $\mu\text{g/L}$. Al³⁺ ions showed LOD of
377 7.6 mM and 200 $\mu\text{g/L}$ for drinkable H₂O, as suggested by Environmental Protection Agency. Thus,
378 considering it an excellent instance for the appropriate detection limit of renewable and
379 discriminative sensors by slowing down. With intention of preparing [{Cd₂(syn-dftpmcp) (1,3-

380 BDC)₂]0.5DMF.H₂O]_n, Li et al [72] applied post synthesis photo-dimerization process, while
381 (syn-dftpmcp stands for syn-3,4,12,13-tetrakis(4-pyridyl)-8,17-bisfluoro-1,2,9,10-diethano[2.2]
382 metacyclophane). The results of metal ions detection in CH₃CN demonstrate that in the presence
383 of 1 mM/L Al³⁺ ions solution, PL emission of framework is fully quenched with an LOD of 183
384 µg/L.

385 **3.2. More s-block and d-block metal ions**

386 The identification of metal ions such as Zn²⁺, Ru²⁺, Tl²⁺, Pb²⁺, Ni²⁺, Mn²⁺, Mg²⁺, In³⁺, Ga³⁺, Fe²⁺,
387 Cr³⁺, Co²⁺, Cd²⁺, Ca²⁺, Bi³⁺, Ba²⁺ and Ag⁺ using LMOFs in comparison to previously reported
388 Fe³⁺, Cr³⁺, Cu²⁺, Al³⁺ and Hg²⁺ ions are limited. In addition, such metal ions could be detected
389 with strategies like mechanism response and structure signal, used to implied for redundant metal
390 ions [15-17, 73, 74]. With intention of favorable probing of Pd²⁺ ions, although, the metal ions are
391 redundantly detected following linker metal ions bonding. As a result, greater research into the
392 detection of these metal ions by LMOFs is required due to the environmental threats and harms
393 that these metal ions cause to humans, as well as the development of information about LMOFs in
394 metal ions detection.

395 **3.3. Detection of metal ions from lanthanide series**

396 Unlike the non-radiative d-d transitions in (d)-LMOFs, the f-f transitions in Ln³⁺ ions are radiative
397 if Ln³⁺ ions centers are effectively sensitized through the antenna effect of the organic ligand and
398 the LMREnT process occurs. Depending upon the unique emission maxima of Ln³⁺ ions, enhanced
399 photoluminescence results in proficient LMREnT. Succeeding post-synthesizing Ln³⁺@MOF-
400 composites, the fundamental factor leading to sensitize Ln³⁺ ions, probing metal ions and emissive
401 character of (f)-LMOFs was supposed to be REnT. Furthermore, the metal ions linking,
402 exchanging cation, configuration breakdown and overlapping manners that are responsible for 1-

403 dimensional improvement or diminishing of λ_{\max} of transduced signal, adopted by (f)-LMOFs
404 employed to sense metal ions. On account of proficient MOF-to- Ln^{3+} -REnT, 1-dimensional turn
405 on the character of specific max of Ln^{3+} ions would be responsible for signal generation after
406 application MOFs to sense Ln^{3+} ions. Because of this reason, Sm^{3+} , Dy^{3+} , Tb^{3+} and Eu^{3+} ions were
407 scrutinized out of Ln^{3+} ions series. With the application of UV light, colorimetric recognition and
408 1-dimensional turn-on stimulation could be observed concurrently. As mentioned above, the color
409 variation in MOF to Ln^{3+} ions could be observed bare eye under UV radiation source unveiling
410 their sensitivity, e.g., Sm^{3+} ions showed orange, Dy^{3+} ions displayed blue, Tb^{3+} ions were detected
411 with green and Eu^{3+} ions were observed with red color. The appearance shade of sensing agent
412 alters after interaction of MOFs and Ln^{3+} ions such as Eu^{3+} ions show red color [75], Tb^{3+} ions
413 give green [76], Dy^{3+} ions exhibit blue [77] and Sm^{3+} ions unveil orange color [77]. On the other
414 hand, fabrication of Ln^{3+} @MOF-composites has been widely administered for the identification
415 of varied samples following an efficient approach of sensitizing Ln^{3+} ions. Free functional-ligands
416 co-ordinational manner, inter-change of anions from a porous framework with cations and pores
417 impregnation with Ln^{3+} ions are the most practiced procedures for preparation of Ln^{3+} @MOF-
418 composites for sensitizing Ln^{3+} ions and application of MOFs for Ln^{3+} ions identification.
419 Comprehensively, high proficiency has been acquired with furnishing suitable factors for sensing
420 and identification of Ln^{3+} ions [77].

421 **4. Nanocomposite based optical sensors**

422 The fluorescent nanosensors have been placed in fascinating class of molecular devices for the
423 detection of various heavy metals in the environment. Various organic dyes such as rhodamine,
424 fluorescein and cyanine are being utilized as fluorescent probes in the sensors. Although, a limited
425 excitation spectrum, little signals, low absorption coefficients, less stability and photo bleaching

426 are associated disadvantages [78]. During the excitation process, the dyes exhibit robust phototoxic
427 impacts to create ROS. The basic simple principle of fluorescence sensors is constructed upon
428 particular interaction between the target analyte (metal ion) and detection component
429 (nanomaterial) to initiate alterations in the fluorescence features of nanomaterial [79]. Recently by
430 employing the different nanomaterials the fluorescence sensors have been developed with
431 enhanced selectivity and sensitivity along with nanocomposite synthesis and functionalization
432 with linkers which may be organic. Nanomaterials improved the identification range, on-site
433 identification potential, stability and also efficient performance of fluorescent based sensors [80].
434 The biomolecules existing on nanomaterial surface help binding of the analyte. The NM-metal
435 ions interactions are commonly concerned with direct fluorescent quenching or energy
436 transference phenomena (FRET, PET, NSET) that lead to the detection of analyte [4, 11, 81].
437 Many fluorescent nanomaterials such as MOFs, polymer dots, carbon quantum dots (CQDs),
438 semiconductor quantum dabs (QDs), silver nanoclusters (AgNCs), gold (AuNCs), up-conversion
439 NPs (UCNPs), and metallic NPs explored for metal ions sensors development.

440 **4.1. Metal NPs and CNTs based sensors**

441 The employment of various nanoparticles (UCNPs, metallic nanoparticles etc.) in fluorescent
442 sensors for the identification of heavy metal ions has attained more attraction because of high bio-
443 compatibility, great specificity, facile synthesis, functionalization of surface and optical properties
444 [50, 82]. Features associated with metallic nanoparticles made them ideal for the development of
445 fluorescent probes with a potential optical array [83]. For the identification of Pb^{2+} ions, many
446 fluorescent nanoparticles have attained attention. For example, in the existence of Pb^{2+} ions, the
447 CuNPs templated with poly-thymine (poly-T) displayed quenching [84]. With great selectivity
448 against other various metal particles in ideal conditions, the nanosensor exhibited a LOD of 0.4

449 nM along with a fast identification time (~10 min). This process proved authenticated with tap
450 H₂O along with a recovery of 99.1%.

451 Similarly, label free procedure established by employing the DNA template CuNPs as fluorescent
452 nano-probes for the identification of Pb²⁺ ions [85]. During the NPs synthesis, it was demonstrated
453 that CuNPs were stabilized by dsDNA encased by Cu²⁺ ions. Metallophilic reactions resulted
454 between Cu²⁺ and Pb²⁺ by the addition of Pb²⁺ ions existing at CuNP surfaces, in this manner
455 inducing fluorescence quenching. With the enhancing Pb²⁺ ions concentration within a range of 5-
456 100 nM (LOD = 5 nM), the fluorescence intensity of NPs reduced. Further, biosynthesized silver
457 nanoparticles were used as fluorescent nano-probes for the advancement of turn-on type Pb²⁺ ions
458 sensors in water [86]. Moreover, functionalized silver nanoparticles with the organic compounds
459 served as an excellent sensing site for metal ions identification. For instance, silver nanoparticles
460 that are modified with catechin are utilized for the formation of a more specific fluorescent Pb²⁺
461 ions sensor [87]. The presence of hydroxyl moieties in catechin initiate the reduction of gold
462 chloride (AuCl₄⁻) ions to produce gold-based nanoparticles. However, on the introduction of Pb²⁺
463 ions to the matrix, the complexes of Pb²⁺-Au and Pb²⁺-catechin were being developed on the gold
464 nanoparticles surface because of electron rich hydroxyl moieties and this enhanced the catalytic
465 potential of gold-based nanoparticles similar to peroxidases. For instance, in the existence of H₂O₂
466 the oxidized amplex ultra red (AUR) probe exhibited the robust intensity of the fluorescence. A
467 linear relation between AUR intensity and Pb²⁺ ions concentration with LOD of 1.5 nM was
468 exhibited by H₂O₂-Catechin-AUR-AuNP probe. Gold based nanoparticles (AuNPs) were being
469 utilized in association with Brilliant Cresyl Blue (BCB) dye for the formation of a FRET-based
470 fluorescent nano-sensor in the near infrared range [88]. The restoration of BCB dye fluorescence
471 occurs because of dye molecules detachment from the gold-based nanoparticles that occurs due to

472 the addition of the Pb^{2+} ions. At optimum conditions, the chelation reaction happened between
473 glutathione capped gold nanoparticles and Pb^{2+} ions. The Pb^{2+} ions concentration could be
474 identified by the nanosensor in the range of 0.16 to 2.1 ng/mL. The nanosensor showed great
475 sensitivity and insignificant interference because of absorbance in NIR region. Gold nanoparticles
476 have been employed as significant fluorescence quencher in NSET method because they have
477 capability to multiply the transfer of energy process [89, 90].

478 For the optical identification of metallic ions (Pb^{2+} and Hg^{2+}), the gold nanoparticles are used in
479 the conjugation with aptamers. The linear relationship between the concentration of these ions and
480 fluorescence intensity was exhibited in the range of 10 pM to 1 μM . Furthermore, the LOD of 27
481 pM for Pb^{2+} and 51 pM for Hg^{2+} was calculated by using the equation $3\sigma/\text{slope}$ in 10 mM sodium
482 phosphate buffer. On the other hand, the LOD for Pb^{2+} and Hg^{2+} in human blood serum was as
483 low as 128 pM and 121 pM respectively [91]. To enhance the selectivity and sensitivity of the
484 fluorescent nanosensors, the employment of up-conversion nanoparticles (UCNPs) doped with the
485 metal/lanthanide ions attracts a great amount of attention during the last decades. Up-conversion
486 nanoparticles have displayed excellent photo-luminescent characteristics through the following
487 mechanism of dual/multi-photon. Further, these have capability to transform longer wavelengths
488 to shorter wavelength fluorescent emissions [92]. In FRET-based Pb^{2+} ions nanosensor, the up-
489 conversion nanoparticles of NaYF_4 functionalized with the ethylene-imine polymer and gold
490 nanoparticles capped with the 11-mercaptoundecanoic acid (MUA) utilized as acceptors and
491 donors respectively [93]. The mechanism of identification is based upon ions chelation that
492 detached Up-conversion NPs from gold nanoparticles in the existence of the Pb^{2+} ions which
493 results in donor fluorescence restoration. With the LOD of 20 nM, the linear identification limit
494 for the established sensor was described as between 0.5 to 10 μM .

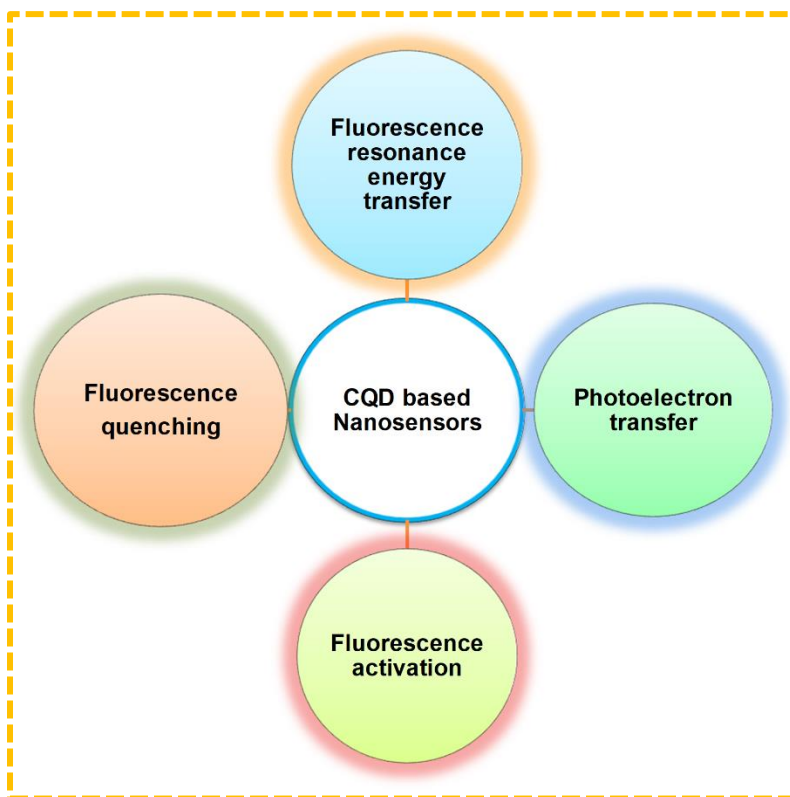
495 Based on gold nano rods (AuNRs) and NaYF₄: Yb, Ho up-conversion nanoparticles, the dual
496 FRET based apta sensor was being formed for the identification of the metal ions [94]. Firstly, the
497 up-conversion nanoparticles improved with amino (-NH₂) moiety associated aptamers through
498 covalently bond and gold nanorods functionalized with thiol-modified corresponding DNA
499 sequences of the Pb²⁺ ions specific DNAzymes. The up-conversion fluorescence (green and red)
500 of UCNPs was quenched because of instantaneous overlapping between absorption spectra of gold
501 nanoparticles and fluorescence emission spectra of up-conversion nanoparticles. Up-conversion
502 fluorescence was restored by the introduction of the Pb²⁺ ions to the matrix, because of the
503 development of G-quadruplex structure between the Pb²⁺ ions and aptamers. Between Pb²⁺ ions
504 concentration and nanoparticles fluorescence intensity, the enhanced linear relationship was
505 observed within the range of 0.1-100 nM (LOD = 50 pM). By utilizing the human blood serum
506 samples and the environmentally polluted food samples, the nanosensor was examined with a
507 restoration value between 96 and 110.6% [94]. Recently for Pb²⁺ ions identification, the
508 NaYF₄/Yb³⁺/Tm³⁺ UCNPs were used as FRET donors while TGA capped CdTe QDs employed as
509 FRET acceptors in nanosensors [95]. The advanced system identified Pb²⁺ ions in human serum
510 with great capability to overcome the auto-fluorescence of serum with LOD of 80 nM. For the
511 identification of Pb²⁺ ions, the fluorescent probes such as AuNCs, AuNRs and AgNCs utilization
512 are the point of interest these days [96-99]. For example, based on fluorescence quenching the
513 glutathione functionalized gold nanorods have been reported for selective Pb²⁺ ions sensing [100].
514 The nanosensor exhibited great sensitivity in an array of 5 nM to 5 mM with LOD of 2 nM. In the
515 same way as a ratiometric fluorescent probe for the identification of Pb²⁺ ions, a hybrid of SiNPs
516 connected with AuNCs/QDs was utilized [101]. Based on ratiometric intensity (I₅₂₀/I₆₂₀) with
517 various Pb²⁺ ions concentrations from 0 to 250 nM (LOD = 3.5 nM) the fluorescence quenching

518 capability of the probe was calculated. Polyvinyl alcohol (PVA) strips coated with AuNC/QD
519 hybrid structures are employed for the identification of Pb^{2+} ions in mineral water, seawater,
520 ground water and tap water. A metal ion identification range of $0.1 \mu M$ was shown by the solid
521 sensor strip [101]. Similarly, for the identification of Pb^{2+} ions in living cells the glutathione (GSH)
522 capped fluorescent silver nanoclusters (AgNCs) have been reported [102]. The identification was
523 based on quenching (fluorescence) because of the coordination connections between Pb^{2+} ions and
524 carboxy/amino moieties existing on GSH-AgNCs (LOD = 0.2 nM). Silver nanoclusters have been
525 templated with the $PS_2.M$ -DNA to form a Pb^{2+} ions nano-biosensor [102]. Fluorescence was
526 enhanced by the introduction of Pb^{2+} ions into the sensor via G-quadruplex development from
527 aptamer-DNA. The two dark AgNC-DNAs situated at 3' and 5' terminals exhibited fluorescence
528 and these were produced due to alteration in DNA-aptamer conformation. With LOD of 3 nM , the
529 higher sensitivity was shown by the nanosensor in the range of 5 to 50 nM . For selectively
530 identifying the Pb^{2+} ions, recently the gold nanoclusters capped with the MPA and GSH have been
531 produced by employing core-etching and ligand change reaction [103]. Big clusters of non-
532 luminescent gold nanoclusters have been produced due to aggregation of gold nanoclusters as well
533 as the interaction between Pb^{2+} ion and thiol moiety present on surface of gold nanoclusters. In
534 natural drinking water, the sensor has LOD of 10 nM . In the identification of metal ions, the CNTs
535 also described as an outstanding fluorescence quencher other than metal nanoparticles [104]. For
536 example, for formation of multi-plexed aptamer metal ions identification system the fluorescence
537 quenching features of multi-walled carbon nanotubes (MWCNTs) were being utilized [105] and
538 system exhibited the LOD of 20 nM . For higher sensitive Pb^{2+} ions sensing, the CNTs
539 functionalized by ATTO-647 N/aptamers have been developed [106]. With LOD of 0.42 nM , the
540 developed aptasensor exhibited significant sensing of Pb^{2+} ions in tap H_2O and in serum samples.

541 Fluorescent nanosensors behaved as amazing sensing tool for practical applications due to
542 designed nanomaterials.

543 **4.2. Carbon quantum dots (CQDs) based sensors**

544 A very attractive class of fluorescent nanomaterials is the carbon quantum dots (CQDs)/carbon
545 dots (CDs) with many amazing characteristics such as the existence of numerous functionalities,
546 cost-effective, facile preparation, tunable emissions, strong photoluminescence, the potential of
547 surface functionalization, bio-compatibility, good photo-stability and very good water solubility
548 [107]. In sensing various kinds of heavy metal ions like Zn^{2+} , Cr^{6+} , Ni^{2+} , Cd^{2+} , Cu^{2+} , Fe^{3+} , Se^{4+} ,
549 As^{3+} , Hg^{2+} and Pb^{2+} ions the CQDs are being employed extensively [108, 109]. Biocompatible and
550 non-toxic CQDs are obtained from natural carbon resources [110]. The general detecting
551 mechanisms of CQD sensors are fluorescence quenching, fluorescence activation, PET, FRET and
552 inside filter effect (Fig. 6).



553

554 **Fig.6.** General Mechanistic approach of CQDs based nanosensors for sensing of metal ions.
555 For example, in chocolate, H₂O soluble fluorescent CQDs are produced by single step hydro-
556 thermal reaction [111]. The prepared CQDs based sensor is employed for the detection of Pb²⁺
557 ions. Great sensitivity was exhibited by nanosensor because of fluorescent quenching that was
558 based on an interaction between Pb²⁺ ions and hydroxyl moieties upon the CQDs. For Pb²⁺ ions
559 detection, the CQDs prepared from the *Osmium Sanctum* were also utilized [112]. Fluorescence
560 of CQDs is greatly quenched in the presence of Pb²⁺ ions because of electron transference (non-
561 radiative) in which amine moiety existing on surfaces of CQD interacted with Pb²⁺ ions (empty d-
562 orbitals). In the same manner, the preparation of nitrogen-doped CQDs was carried out by
563 employing the *Lantana camera* berries (as a source of carbon) and for the doping agent, EDTA
564 was used [113]. In human serum and real water samples, the CQDs (QY= 33.15%) were being
565 utilized as an amazing sensing agent for the identification of Pb²⁺ ions with the sensing limit from
566 0 to 200 nM with 9.6 nM LOD. The *Gingko biloba* leaf extracts were utilized for the derivation of
567 flavonoid doped CQDs these were used for the development of a Pb²⁺ ions sensor [114]. Flavonoid
568 glycosides present on the surface of CQDs were being specifically bonded by Pb²⁺ ions and this
569 led to fluorescence quenching. With a LOD of 55 μM, the Pb²⁺ ions detected by the nanosensor
570 were within the 1-20 nM range. Through dipole-dipole force and hydrogen bonding, the agarose
571 hydrogel was further used for flavonoid-CQDs doping to develop a detecting system. With 12.89
572 nM LOD the gel slices were utilized for the removal and identification of Pb²⁺ ions [114]. For
573 fluorescence and colorimetric-based Pb²⁺ ions sensing in water samples, the fabrication of the
574 CQDs with table sugar was carried out [114]. Turbidimeter was employed to quantify the Pb²⁺
575 ions concentration with excellent selectivity (LOD = 14 μg/L) that was close to the permissible
576 limit of Pb²⁺ ions in drinking H₂O (15 μg/L). Similarly, the dextrose ager also known as biological
577 media was employed for the carbon nano-rods preparations through microwave heating for the

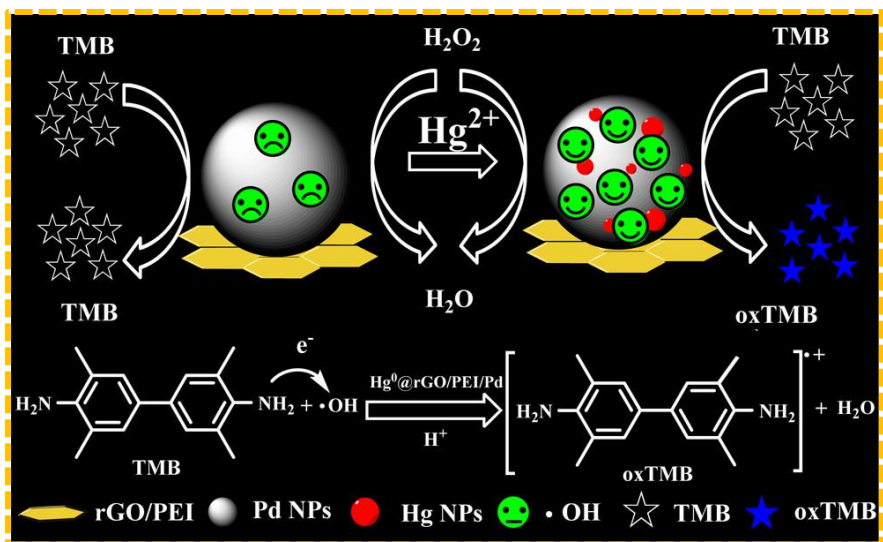
578 formation of an effective lead sensor [115]. The multicolor fluorescence was exhibited by the
579 multicolor CQDs and water-soluble CQDs. Pb^{2+} ions developed a complex by coordinating with
580 hydroxyl and carboxylic moieties existing upon CQDs surface that initiate the fluorescence
581 quenching via PET mechanism (with LOD 0.73 nM and 1.1 nM in tap water samples and river
582 water samples respectively [116]. On the cellulose paper strips the CQDs were additionally
583 embedded that exhibited the identification limit of 106 μM [115, 116]. For Pb^{2+} ions sensing in
584 aqueous solution, the chemically prepared CQDs were also utilized. Nitrogen doped CQDs (N-
585 CQDs) were synthesized using glycerol and EDTA (under microwave radiations exhibiting LOD
586 of 0.1-6 μM [117]. Fluorescent CQDs were synthesized using bovine serum albumin protein
587 through single step method (LOD = 5.05 μM) [118]. Conjugation of N-CQDs was done with
588 magnetic NPs (Fe_3O_4 nanoparticles) for the identification and adsorption of Pb^{2+} ions [118]. For
589 the pre-concentration and solid-phase extraction of Pb^{2+} ions from vegetative samples and H_2O
590 samples, N-CQD/ Fe_3O_4 NP hybrid adsorbent material was utilized. The presence of functional
591 moieties (hydroxyl, carboxylic and C-O-C-) on CQDs permitted great Pb^{2+} ions adsorption during
592 extraction with an identification range of 0.3 to 300 $\mu g/L$ [39]. Moreover, for the development of
593 a turn-off/on Pb^{2+} ions sensor the CQDs were also utilized. Thus, for the instantaneous
594 identification of pyrophosphate (PPi) and Pb^{2+} ions, highly fluorescent and water-soluble CQDs
595 were obtained from kerosene soot [119]. The interaction of Pb^{2+} ions with carboxyl moieties
596 existing on the surface of CQDs lead to reduce the CQDs intensity of fluorescence. By
597 incorporation of PPi in the system, fluorescence was regained because of the great binding
598 capability to Pb^{2+} ions than CQDs. With LOD of 2 nM, the Pb^{2+} ions were identified in the range
599 of 0.5 to 11 μM . By utilizing the sodium-citrate and poly-acrylamide (precursors) the blue
600 fluorescent CQDs were prepared for the advancement of “turn-off/on” Pb^{2+} ions sensor with a

601 detection limit of 4.6 nM [120]. For the development of “turn-off/on type” Pb^{2+} ions sensor, boron
602 doped CQDs are reported [121]. The chelation between Pb^{2+} ions and oxygen atoms existing on
603 the surface of CQD forms complex (non-fluorescent) with DL of 25 to 250 μM . The N-CQDs
604 acquired from pyrolysis of citric acid and ethanol-amine have been demonstrated for the formation
605 of “turn-on” type Pb^{2+} ions sensor [122]. Initially, due to interaction (electrostatic) between the
606 carboxyl moieties of PAAs and amino groups of CQDs (range 0-1.67 mM and LOD of 22.8 μM),
607 the fluorescence of immobilized CQDs (at λ_{max} 430 nm) was quenched. For the identification of
608 bio-molecules, analytes and metals, CQD based ratiometric fluorescent method have been
609 employed [70]. Through solvothermal process, the multiemissive CQD hybrids were synthesized
610 from bamboo leaves [70]. Hybrids of CQDs were synthesized in existence of sodium carbonate to
611 acquire triple emissive CQDs at a single wavelength of 400 nm. The Pb^{2+} ions interacted with
612 flavonoid moieties existing on surface of CQD with quenching fluorescence of CQDs @ 493 nm
613 and improved signal @ 653 nm. The fluorescence response plotted against Pb^{2+} ions concentration
614 to get detection range from 0.6 to 800 nM (with LOD of 0.14 nM). In another study, CQDs were
615 produced by utilizing the glutathione and formamide under microwave method by employing a
616 ratiometric fluorescent sensing system [123]. The CQDs (QY 6.49%) exhibited fluorescence and
617 absorption both in blue and red spectral regions at the same time. The interactions between the
618 Pb^{2+} ions and surface groups (-COOH, C=N, C=S) of the CQDs are driven to such fluorescence
619 quenching. With a LOD of 37.1 nM, the double fluorescent CQDs exhibited a greater sensitivity
620 within linear range (1-961 nM). For FRET-based identification of Pb^{2+} ions, another ratiometric
621 fluorescent sensor was created utilizing amino capped CQDs and the GSH-functionalized gold
622 nanoclusters (AuNCs) [124]. The CQDs (positively charged) served as energy donor and gold
623 nanoclusters (negatively charged) employed as energy acceptors and both of these were utilized

624 as FRET pair in research work. When excited at a wavelength of 380 nm the fluorescent probe
625 exhibited double crests at 440 and 565 nm. The introduction of Pb^{2+} ions enhanced the gold
626 nanoclusters fluorescence while this did not affect the CQDs. This happened because thiolated
627 gold nanoclusters exhibited photo-luminescence on their aggregation [125]. Within the limit of 2
628 to 60 μM and with an LOD of 0.5 μM , the created ratiometric sensor showed a direct relationship
629 between Pb^{2+} ions concentration and probe ratiometric intensity (I_{565}/I_{440}). In view of these
630 improvements and a broad ubiquity of CQDs as a lead detecting material, it could be concluded
631 that environment friendly CQD-based sensing probes will coordinate with simpler readout
632 frameworks and imaging helped quantification strategies in the future.

633 **4.3. Nanocomposites for colorimetric responses**

634 Nanoparticles such as gold, silver and lead have peroxidase mimetic potential and the gathering of
635 these nanoparticles with graphene can increase their stability, in addition, provide them with
636 excellent catalytic potential. By utilizing this characteristic, several sensors for heavy metal ions
637 have been proposed. It was evident that GO-AuNP nanohybrids with peroxidase type potential
638 would distinguish between the single and double-stranded deoxy-ribonucleic acid (DNA) and then
639 Pb^{2+} , Hg^{2+} ions could be colorimetrically identified based on the metal ion activated DNA
640 conformation development [126]. According to a research report, the existence of Hg^{2+} could
641 increase and improve the peroxidase mimetic potential of reduced graphene oxide/poly-
642 ethyleneimine/palladium-nanoparticles (rGO/PEI/Pd) nanohybrids enhancing the oxidation and
643 color variation of 3,3',5,5'-tetra-methylbenzidine in solution and recognizing selective
644 identification of Hg^{2+} ions with LOD of 0.39 nM (Fig. 7) [127].

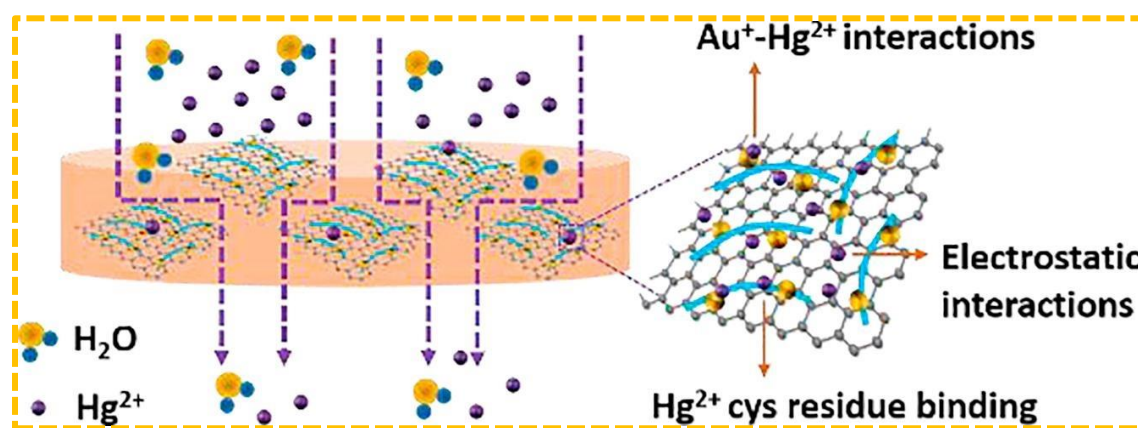


645
 646 **Fig. 7.** Mercury-enhanced peroxidase-like activity of rGO/PEI/Pd nanohybrids and reaction
 647 principle. This figure is obtained with permission from Ref. [127].

648 Zhi and coworkers [128] made graphene-doped MoS₂ aerogels to support Au/Fe₃O₄ nano-
 649 particles. Fe₃O₄ nanoparticles bestowed magnetic features to aerogels. The prepared nanohybrid
 650 materials facilitate facile reusability and recovery of catalyst. Further, the detection was supported
 651 by the addition of gold nanoparticles in an aqueous medium. The formed Hg²⁺ ions contained
 652 aerogel that stimulated peroxidase mimetic potential. In addition to the per-oxidase mimetic
 653 potential, upon introduction of Hg²⁺ ions the direct solution color change of the nanocomposites
 654 has also been referred to as the detection of Hg²⁺ ions. By following a simple one-pot oxidation-
 655 reduction reaction, Yan and his colleagues [129] prepared multi-functional graphene gold
 656 nanocomposites (G-AuNPs). The formed G-AuNPs initiate a colorimetric change upon
 657 introduction of Hg²⁺ ions from purple red to brown in the presence of ascorbic acid. These
 658 colorimetric changes owe the formation of an amalgam of AuNPs enabling the naked eye
 659 identification of Hg²⁺ ions.

660 **4.4. Nanocomposites for fluorescent detection**

661 Graphene oxide and graphene have been used (as substrate) for loading of fluorophore through
662 direct assembling of fluorescent nanoparticles or by employing biomolecules to capture the
663 fluorophores. The simultaneous removal and identification of Hg^{2+} ions was carried out using rGO-
664 Fe_3O_4 functionalized with Hg^{2+} ions specific T-DNA [130]. In another study, the detection of Hg^{2+}
665 ions with double-gold nanoclusters/graphene oxide (D-GNCs/GO) has been reported via
666 electrostatic interactions, where D-GNCs enhance the detection sensitivity and graphene oxide can
667 stimulate the rate of reaction [131]. Graphene oxide decorated with AuNCs@BSA is employed
668 for the identification and isolation of Hg^{2+} ions based on the metal binding characteristic of
669 AuNCs@BSA nanofibers and large surface area of graphene oxide. It was assumed that the high
670 separation effectiveness of the hybrid membrane can be ascribed to the uncommon Hg^{2+} - Au^+
671 interactions, Hg^{2+} -cysteine residue binding, and the hybrid membrane (Fig. 8) [132]. Liu et al.
672 [133] adjusted graphene oxide with Ag-In-Zn-S quantum dabs (QDs). The addition of Cu^{2+} ions
673 would initiate the accumulation of QDs and consequent fluorescence quenching can be utilized for
674 Cu^{2+} ions assurance.



675
676 **Fig. 8.** Adsorption mechanism in the stacked sheets of GO-AuNCs@BSA nanofibers hybrid
677 membrane. This figure was obtained with permission from Ref. [132].

678 4.5. Nanocomposites as fluorescence quenchers

679 Dye-labelled ssDNA by hydrophobic and π - π interactions may be well adsorbed by graphene
680 oxide and at the same time quench the fluorescence of dyes resonance by FRET, whereas dsDNA
681 or other DNAs are not able to bind to the surface of graphene oxide. These features made graphene
682 oxide an attractive and efficient DNA based fluorescent sensing system for the identification of
683 heavy metal ions. FRET/shell-insulated metal nanoparticle surface-enhanced fluorescence
684 spectroscopy (FRET/SIMNSEF) protocol having graphene oxide and anisotropic shell-insulated
685 metallic nanoparticles (SIMNs) demonstrated for the sensing of Hg^{2+} ions by T-rich ssDNA
686 functionalization. While the absence of Hg^{2+} ions, fluorophore-labelled ssDNA adorned on SIMNs
687 adsorb on the surface of graphene oxide and thus the fluorescence could be quenched by the FRET.
688 DNA hairpin framework formation is due to THg^{2+} -T coordination. Furthermore, the decreased
689 interaction between the graphene oxide and DNA provides ultimate fluorescence restoration and
690 further the surface enhanced fluorescence (SEF) effect increase and amplify the fluorescence
691 signal, realizing the sensitive identification of Hg^{2+} ions [134]. Two hairpin probes and a helper
692 DNA have been designed and these could be adsorbed on graphene oxide to quench the
693 fluorescence of the label. The hybridization chain reactions (HCRs) between the two hairpin
694 probes started through the Hg^{2+} ions employing the helper DNA by T- Hg^{2+} -T coordination
695 chemistry. The dsDNA products were released from the graphene oxide and the fluorescence was
696 restored. The methodology can be applied in sensitive Hg^{2+} ion sensing with a LOD of 0.3 nM
697 [135].

698 Similarly, Hg^{2+} (Ag^+ , Pb^{2+}) ions sensing platforms have been constructed based on fluorescence
699 variation because of conformation DNA development on combining with Hg^{2+} (Ag^+ , Pb^{2+}) ions to
700 create the T- Hg^{2+} -T (C-Ag^+ -C, Pb^{2+} -G-quadruplex) base pairs [136-138]. The sensing platforms
701 for Hg^{2+} and Pb^{2+} ions identification have been proposed on basis of quenching nanoparticles

702 fluorescence [139, 140]. As a linker to bridge graphene oxide and GQDs another distinctive
703 technique utilized Grich DNA and after that to initiate the formation of G-quadruplex the Pb^{2+} ions
704 were utilized. Leading to the shortening of the distance between graphene oxide and GQDs leading
705 to an alteration within the chain length, in this way fluorescence quenching was observed in GQDs
706 and this happened due to energy transfer between graphene oxide and GQDs [141]. Metal ion
707 specific DNazymes have been utilized for the construction of the detecting platform. Liu and his
708 colleagues [142] reported the Cu^{2+} ions dependent DNzyme having a 30-FAM-developed Cu-
709 Sub and a Cu-Enzyme can be gathered with graphene, resulting in close proximity of fluorophore
710 to the surface of graphene to assist the complete quenching. The self-gathered graphene DNzyme
711 configuration disturbed by the proximity of Cu^{2+} ions would cleave the DNA substrate hence
712 discharging FAM-labeled DNA strand to produce increased Cu^{2+} ions concentration dependent
713 fluorescence signals. FAM-labeled were also replaced by fluorophore [143]. For the examination
714 of Pb^{2+} ions, the DNzyme principle was implemented [144]. To create an inflexible structure
715 with little ssDNA circles they utilized Pb^{2+} ions dependent 8-17 DNzymes to hybridize with the
716 Cy3-labeled substrate that might not tie effectively to graphene oxide, and in this way, the
717 fluorescence of Cy3 might not be quenched. Upon Pb^{2+} ions addition, the Cy3- labelled part was
718 discharged and 17S substrate strand was cleaved, leading to the strong quenching of the
719 fluorescence flag by graphene oxide. The obtained results were controversial [145]. Different
720 fluorescence responses in reference [145] may be due to various lengths and configurations of
721 DNzyme-substrates and different affinities of discharged fragments to graphene/graphene oxide.
722 Molecular beacon (MB) having fluorophore and a quencher in near vicinity with quenched
723 fluorescence and furthermore the graphene oxide adsorption can reduce the back-ground
724 fluorescence. The Cu^{2+} ions and H_2O_2 existence may break the molecular beacons into small

725 portions that can be released from surface of graphene oxide which restores the Cu^{2+} ions
726 dependent fluorescence [146].

727 **4.6. Probing through fluorescent nanoclusters**

728 Surface-layer of rGO was passivated and its FL intensified after improvement with T following
729 SN^2 methodology, demonstrated by Dinda and coworkers [147]. Grounding on Thymine- Hg^{2+} -T
730 communication, Hg^{2+} ions recognition has been tripped by applying the thermally reduced
731 graphene oxide as a fluorescence detector. On the account of elevated bonding fascination of Hg^{2+}
732 and I^- ions, the I^- ions could be identified with greater ease. A remarkable refurbishment and
733 revamping in the fluorescence of graphene was proposed by Fu and coworker [148] that in the
734 existence of $\text{S}_2\text{O}_3^{2-}$ and $\text{HOCH}_2\text{CH}_2\text{SH}$, Pb^{2+} ions increased the percolating speed of gold-NPs that
735 in-turn was produced quenching of graphene fluorescence intensity. Moreover, mineral water and
736 tap water specimens are also supplied with the same sensor for estimating Pb^{2+} ions. Ag^+ and Hg^{2+}
737 ions sensing has also been acquired with the nearness of these ions transferring electrons between
738 these ions and graphene oxide, like customary fluorescence -NPs e.g., semiconducting quantum
739 dots. The fluorescence quenching owing to electron transfer among heavy metal ions and graphene
740 oxide succeeding evolution of double-stranded DNA with a hairpin appearance that emerged after
741 particular $\text{Hg}^{2+}/\text{Ag}^+$ ions adhering to single-stranded DNA (T-rich/C-rich) preceding its
742 functionalization on the surface of graphene oxide [148, 149]. For the manufacturing of nano
743 compounds with dual radiance characteristics, semiconducting quantum dots were aided via GO
744 displaying efficient fluorescence and were introduced by Li et al. [149]. It is advantageous in
745 discriminative and responsive detection of Cu^+ ions [149]. Advantageously, responsive and
746 discriminative ascertainment of Cu^+ ions has been achieved through observing its effect on NCs

747 fluorescence red glow turning blue and red colored fluorescence emission of quantum dots got
748 quenched while graphene oxide underwent no change in fluorescence shade.

749 **5. Differentiation between orthodox sensors and nano-sensors**

750 Inorganic precursors with non-poisonous, cost-effective and bio-suitable in nature are used to
751 prepare nanomaterials supported probes in contrast to traditionally employed probes. Virtually, such
752 probes have been fascinated because of facile synthetic procedures and potential implications,
753 inexpensiveness and increased LOD. For modelling and preparation of optical sensors, NMs are
754 used as excellent translating-section due to their distinguishing characteristics. Furthermore,
755 optical characteristics of NMs were arrayed by target-initiated aggregation/anti-aggregation and
756 surface improvement [32, 52]. In addition, optical sensors of nano substances were analyzed with
757 smaller sized ligands/macro-biomolecules being the identification module. Particular and
758 distinguished sensing of heavy metal ions was also possible with the detection section that
759 furnishes the target specimen with unique biological and chemical interactions. Moreover, swift
760 qualitative/quantitative sensing of heavy metals with greater selectivity in comparison to
761 colorimetric detectors has been achieved using luminescence-based nanoparticles. On contrary,
762 some of the disadvantages related to the aqueous detections and biologically active metal ions
763 detection were noticed on the rounds of poor water solubility, toxicity and inappropriateness of
764 orthodox photoluminescent organic dyes like organic fluorophores and emissive conjugated-
765 polymers [150]. For apprehending organic luminescence, a detailed overview of the structure and
766 synthetic pathways of the compound must be known in comparison to luminescent nanoparticles.
767 Photobleaching of organic dyes could happen even with facile observation and elevated
768 susceptibility. The photo-bleaching of organic chromophores is repressed by Raman sensors.
769 However, electromagnetic amplification causes Raman scattering remarkably effective when poor

770 efficiency was faced. Therefore, SERES and LOD could proficiently be improved with
771 standardization of constitution, volume and configuration of plasmonic nano-structures [151].
772 Furthermore, the implementation of nanomaterials as sensing modalities has greatly improved the
773 sensing abilities of chemosensors. In an aqueous solution, the distinctive identification of Cu^{2+} and
774 Hg^{2+} ions were achieved through immobilization of emissive dipeptidyl chemosensor (DPN) over
775 silicon nanoparticles generating SiNPs@DPN by Chung and his coworkers [91]. Conjugation of
776 MSiNPs with DPN remarkably enhanced LOD up to 96 nM for Hg^{2+} ions. Metallic ions in lower
777 amounts were ascribed to nanoparticles triggering signal enlargement. Likewise, 0.768 μM LOD
778 was observed for discerning Cu^{2+} ions under chemosensor radiant of rhodamine B [152].
779 Nevertheless, an upgraded LOD of less than 0.3 mg/L and boosted response for probing Cu^{2+} ions
780 in the solution state was exhibited by surface modified MSNPs with rhodamine implanted through
781 covalent bonds. Noticeable implications are discerned for lab on chip technology and bioimaging
782 owing to efficient regenerative ability and resilience of hybrid-substance. Macro-biomolecules and
783 micro-molecular ligands were employed probing agent for contrasting organic fluorescent
784 nanosensors and chemosensors.

785 **6. Conclusion and future prospects**

786 The necessity of unique tools for real-time detection of diverse water contaminants is generally
787 recognized around the world. This review offered a critical appraisal of recent advances in a real-
788 time monitoring system, based on the fluorescent, luminescence and colorimetric detection
789 methods. The focus of this review was to present the advancement in nanomaterial-based
790 nanosensors for sensing heavy metal ions in aqueous matrices with enhanced selectivity, efficacy
791 and sensitivity. Sensors exhibited better sensitivity and selectivity with the incorporation of
792 nanomaterials. In a comparison of conventional sensors, nanomaterial-based sensors are found

793 preferable because of facile synthesis, lower LOD values and cost-effectiveness in various
794 practical applications. Despite significant advancements and developments, the recognition of
795 heavy metal ions by these nanostructures still faces significant developmental problems related to
796 their suitability in real-world samples such as biological and raw water samples. The weak self-
797 stability of nanostructures must be addressed to meet the requirement for heavy metal ions
798 monitoring in complex matrices such as biological samples, wastewater and seawater samples. As
799 a result, new stable nanomaterials must be designed and developed, necessitating the use of novel
800 modification techniques for enhanced functionalization. Additionally, in designing the
801 nanomaterial-based sensors, selectivity must be addressed by selecting suitable binding sites such
802 as specific biological macromolecules or small organic molecules which selectively binds the
803 analytes of major concern. Finally, combining nano-systems with other technologies such as
804 microfluidic or paper chips, as well as test strips, holds a lot of potential for the creation of portable
805 devices that can detect heavy metal ions on a commercial or industrial scale. In conclusion,
806 combining nano-systems with other technologies such as paper chips, microfluidic as well as test
807 strips, holds a lot of potential for the creation of portable devices that can detect heavy metal ions
808 on an industrial or commercial scale

809 **Acknowledgments**

810 The representative Universities or institutes are thankfully acknowledged for providing literature
811 services.

812 **Conflict of interest disclosure**

813 The representative authors have no conflict of interest to disclose in any capacity, either competing
814 or financial.

815 **References**

816 [1] F. Fu, Q. Wang, Removal of heavy metal ions from wastewaters: a review, *Journal of Environmental*
817 *Management*, 92 (2011) 407-418.

818 [2] T. Rasheed, F. Nabeel, C. Li, Y. Zhang, Rhodol assisted alternating copolymer based chromogenic
819 vesicles for the aqueous detection and quantification of hydrazine via switch-on strategy, *Journal of*
820 *Molecular Liquids*, 274 (2019) 461-469.

821 [3] T. Rasheed, F. Nabeel, K. Rizwan, M. Bilal, T. Hussain, S.A. Shehzad, Conjugated supramolecular
822 architectures as state-of-the-art materials in detection and remedial measures of nitro based compounds: a
823 review, *TrAC Trends in Analytical Chemistry*, 129 (2020) 115958.

824 [4] T. Rasheed, F. Nabeel, S. Shafi, Chromogenic vesicles for aqueous detection and quantification of
825 Hg^{2+}/Cu^{2+} in real water samples, *Journal of Molecular Liquids*, 282 (2019) 489-498.

826 [5] T. Rasheed, F. Nabeel, S. Shafi, M. Bilal, K. Rizwan, Block copolymer self-assembly mediated
827 aggregation induced emission for selective recognition of picric acid, *Journal of Molecular Liquids*, 296
828 (2019) 111966.

829 [6] T.H. Zhi-lin Hou, Cai-yun Cai, T. Resheed, C.Yu, Y.Zhou., D.-y. Yan, Polymer vesicle sensor through
830 the self-assembly of hyperbranched polymeric ionic liquids for the detection of SO_2 derivatives, *Chinese*
831 *Journal of Polymer Science*, 35 (2017) 602–610.

832 [7] V. Poornima, V. Alexandar, S. Iswariya, P.T. Perumal, T.S. Uma, Gold nanoparticle-based nanosystems
833 for the colorimetric detection of Hg^{2+} ion contamination in the environment, *RSC Advances*, 6 (2016)
834 46711-46722.

835 [8] I. Ugulu, Determination of heavy metal accumulation in plant samples by spectrometric techniques in
836 Turkey, *Applied Spectroscopy Reviews*, 50 (2015) 113-151.

837 [9] M.S. Gustin, D. Hou, F.M.G. Tack, the term "heavy metal(s)": history, current debate, and future use,
838 *Science of the Total Environment*, 789 (2021) 147951.

839 [10] K. Karim, S. Guha, R. Beni, Comparative analysis of water quality disparities in the United states in
840 relation to heavy metals and biological contaminants, *Water*, 12 (2020) 967.

841 [11] T. Rasheed, M. Bilal, F. Nabeel, H.M. Iqbal, C. Li, Y. Zhou, Fluorescent sensor based models for the
842 detection of environmentally-related toxic heavy metals, *Science of the Total Environment*, 615 (2018)
843 476-485.

844 [12] T. Rasheed, A.A. Hassan, F. Kausar, F. Sher, M. Bilal, H.M. Iqbal, Carbon nanotubes assisted
845 analytical detection–Sensing/delivery cues for environmental and biomedical monitoring, *TrAC Trends in*
846 *Analytical Chemistry*, 132 (2020) 116066.

847 [13] T. Rasheed, C. Li, M. Bilal, C. Yu, H.M. Iqbal, Potentially toxic elements and environmentally-related
848 pollutants recognition using colorimetric and ratiometric fluorescent probes, *Science of the Total*
849 *Environment*, 640 (2018) 174-193.

850 [14] T. Rasheed, C. Li, F. Nabeel, W. Huang, Y. Zhou, Self-assembly of alternating copolymer vesicles for
851 the highly selective, sensitive and visual detection and quantification of aqueous Hg^{2+} , *Chemical*
852 *Engineering Journal*, 358 (2019) 101-109.

853 [15] T. Rasheed, C. Li, F. Nabeel, M. Qi, Y. Zhang, C. Yu, Real-time probing of mercury using an efficient
854 “turn-on” strategy with potential as in-field mapping kit and in live cell imaging, *New Journal of Chemistry*,
855 42 (2018) 10940-10946.

856 [16] T. Rasheed, F. Nabeel, M. Adeel, K. Rizwan, M. Bilal, H.M. Iqbal, Carbon nanotubes-based cues: a
857 pathway to future sensing and detection of hazardous pollutants, *Journal of Molecular Liquids*, 292 (2019)
858 111425.

859 [17] T. Rasheed, F. Nabeel, C. Li, M. Bilal, Rhodamine-assisted fluorescent strategy for the sensitive and
860 selective in-field mapping of environmental pollutant $Hg(II)$ with potential bioimaging, *Journal of*
861 *Luminescence*, 208 (2019) 519-526.

862 [18] M. Arora, B. Kiran, S. Rani, A. Rani, B. Kaur, N. Mittal, Heavy metal accumulation in vegetables
863 irrigated with water from different sources, *Food Chemistry*, 111 (2008) 811-815.

864 [19] J. Briffa, E. Sinagra, R. Blundell, Heavy metal pollution in the environment and their toxicological
865 effects on humans, *Heliyon*, 6 (2020) e04691.

866 [20] B. Kaur, R. Srivastava, B. Satpati, Ultratrace detection of toxic heavy metal ions found in water bodies
867 using hydroxyapatite supported nanocrystalline ZSM-5 modified electrodes, *New Journal of Chemistry*, 39
868 (2015) 5137-5149.

869 [21] X. Yuan, M.I. Setyawati, A.S. Tan, C.N. Ong, D.T. Leong, J. Xie, Highly luminescent silver
870 nanoclusters with tunable emissions: cyclic reduction–decomposition synthesis and antimicrobial
871 properties, *NPG Asia Materials*, 5 (2013) e39-e39.

872 [22] C.V. Hoang, M. Oyama, O. Saito, M. Aono, T. Nagao, Monitoring the presence of ionic mercury in
873 environmental water by plasmon-enhanced infrared spectroscopy, *Scientific Reports*, 3 (2013) 1-6.

874 [23] M. Li, H. Gou, I. Al-Ogaidi, N. Wu, Nanostructured sensors for detection of heavy metals: a review,
875 *ACS Sustainable Chemistry & Engineering*, 1, (2013), 713–723

876 [24] S. Yu, H. Tang, D. Zhang, S. Wang, M. Qiu, G. Song, D. Fu, B. Hu, X. Wang, MXenes as emerging
877 nanomaterials in water purification and environmental remediation, *Science of The Total Environment*,
878 (2021) 152280.

879 [25] S. Yu, H. Pang, S. Huang, H. Tang, S. Wang, M. Qiu, Z. Chen, H. Yang, G. Song, D. Fu, Recent
880 advances in metal-organic framework membranes for water treatment: A review, *Science of The Total*
881 *Environment*, 800 (2021) 149662.

882 [26] S. Zhang, J. Wang, Y. Zhang, J. Ma, L. Huang, S. Yu, L. Chen, G. Song, M. Qiu, X. Wang,
883 Applications of water-stable metal-organic frameworks in the removal of water pollutants: A review,
884 *Environmental Pollution*, 291 (2021) 118076.

885 [27] E. Singh, M. Meyyappan, H.S. Nalwa, Flexible graphene-based wearable gas and chemical sensors,
886 *ACS Applied Materials & Interfaces*, 9 (2017) 34544-34586.

887 [28] S.K. Krishnan, E. Singh, P. Singh, M. Meyyappan, H.S. Nalwa, A review on graphene-based
888 nanocomposites for electrochemical and fluorescent biosensors, *RSC Advances*, 9 (2019) 8778-8881.

889 [29] S.B. Borah, T. Bora, S. Baruah, J. Dutta, Heavy metal ion sensing in water using surface plasmon
890 resonance of metallic nanostructures, *Groundwater for Sustainable Development*, 1 (2015) 1-11.

891 [30] P. Gruber, M.P. Marques, N. Szita, T. Mayr, Integration and application of optical chemical sensors
892 in microbioreactors, *Lab on a Chip*, 17 (2017) 2693-2712.

893 [31] H.H. Qazi, A.B. Mohammad, M. Akram, Recent progress in optical chemical sensors, *Sensors*, 12
894 (2012) 16522-16556.

895 [32] Y. Ding, S. Wang, J. Li, L. Chen, Nanomaterial-based optical sensors for mercury ions, *TrAC Trends*
896 *in Analytical Chemistry*, 82 (2016) 175-190.

897 [33] I. Buryakov, T. Buryakov, V. Matsaev, Optical chemical sensors for the detection of explosives and
898 associated substances, *Journal of Analytical Chemistry*, 69 (2014) 616-631.

899 [34] F. Nabeel, T. Rasheed, Rhodol-conjugated polymersome sensor for visual and highly-sensitive
900 detection of hydrazine in aqueous media, *Journal of Hazardous Materials*, 388 (2020) 121757.

901 [35] F. Nabeel, T. Rasheed, M.F. Mahmood, S.U.-D. Khan, Hyperbranched copolymer based
902 photoluminescent vesicular probe conjugated with tetraphenylethene: Synthesis, aggregation-induced
903 emission and explosive detection, *Journal of Molecular Liquids*, 308 (2020) 113034.

904 [36] Z. Wang, L. Zhang, K. Zhang, Y. Lu, J. Chen, S. Wang, B. Hu, X. Wang, Application of carbon dots
905 and their composite materials for the detection and removal of radioactive ions: A review, *Chemosphere*,
906 287 (2022) 132313.

907 [37] J. Li, J.-J. Zhu, Quantum dots for fluorescent biosensing and bio-imaging applications, *Analyst*, 138
908 (2013) 2506-2515.

909 [38] Y.Y. Wang, X. Xiang, R. Yan, Y. Liu, F.L. Jiang, Förster resonance energy transfer from quantum
910 dots to rhodamine B as mediated by a cationic surfactant: a thermodynamic perspective, *The Journal of*
911 *Physical Chemistry C*, 122 (2018) 1148-1157.

912 [39] J. Ju, W. Chen, Synthesis of highly fluorescent nitrogen-doped graphene quantum dots for sensitive,
913 label-free detection of Fe (III) in aqueous media, *Biosensors and Bioelectronics*, 58 (2014) 219-225.

914 [40] S. Li, Y. Li, J. Cao, J. Zhu, L. Fan, X. Li, Sulfur-doped graphene quantum dots as a novel fluorescent
915 probe for highly selective and sensitive detection of Fe³⁺, *Analytical Chemistry*, 86 (2014) 10201-10207.

916 [41] J. Wang, C. Jiang, X. Wang, L. Wang, A. Chen, J. Hu, Z. Luo, Fabrication of an “ion-imprinting”
917 dual-emission quantum dot nanohybrid for selective fluorescence turn-on and ratiometric detection of
918 cadmium ions, *Analyst*, 141 (2016) 5886-5892.

919 [42] J. Liu, G. Lv, W. Gu, Z. Li, A. Tang, L. Mei, A novel luminescence probe based on layered double
920 hydroxides loaded with quantum dots for simultaneous detection of heavy metal ions in water, *Journal of*
921 *Materials Chemistry C*, 5 (2017) 5024-5030.

922 [43] R. Zhang, W. Chen, Nitrogen-doped carbon quantum dots: facile synthesis and application as a “turn-
923 off” fluorescent probe for detection of Hg^{2+} ions, *Biosensors and Bioelectronics*, 55 (2014) 83-90.

924 [44] B. Paramanik, S. Bhattacharyya, A. Patra, Detection of Hg^{2+} and F^- ions by using fluorescence
925 switching of quantum dots in an Au-cluster–CdTe QD nanocomposite, *Chemistry–A European Journal*, 19
926 (2013) 5980-5987.

927 [45] D. Chen, H. Feng, J. Li, Graphene oxide: preparation, functionalization, and electrochemical
928 applications, *Chemical Reviews*, 112 (2012) 6027-6053.

929 [46] Y.-L. Zhang, L. Wang, H.-C. Zhang, Y. Liu, H.-Y. Wang, Z.-H. Kang, S.-T. Lee, Graphitic carbon
930 quantum dots as a fluorescent sensing platform for highly efficient detection of Fe^{3+} ions, *RSC Advances*,
931 3 (2013) 3733-3738.

932 [47] X. Ran, H. Sun, F. Pu, J. Ren, X. Qu, Ag nanoparticle-decorated graphene quantum dots for label-free,
933 rapid and sensitive detection of Ag^+ and biothiols, *Chemical Communications*, 49 (2013) 1079-1081.

934 [48] Y.-C. Lu, J. Chen, A.-J. Wang, N. Bao, J.-J. Feng, W. Wang, L. Shao, Facile synthesis of oxygen and
935 sulfur co-doped graphitic carbon nitride fluorescent quantum dots and their application for mercury (II)
936 detection and bioimaging, *Journal of Materials Chemistry C*, 3 (2015) 73-78.

937 [49] J. Chang, G. Zhou, E.R. Christensen, R. Heideman, J. Chen, Graphene-based sensors for detection of
938 heavy metals in water: a review, *Analytical and Bioanalytical Chemistry*, 406 (2014) 3957-3975.

939 [50] J.R. Choi, D. M. Shin, H. Song, D. Lee, K. Kim, Current achievements of nanoparticle applications in
940 developing optical sensing and imaging techniques, *Nano Convergence*, 3 (2016) 1-13.

941 [51] E. Singh, H. Nalwa, Nanomaterial-based flexible and multifunctional sensors, in, *American Scientific*
942 *Publishers*, Los Angeles, 2019.

943 [52] M. Sabela, S. Balme, M. Bechelany, J.M. Janot, K. Bisetty, A review of gold and silver nanoparticle-
944 based colorimetric sensing assays, *Advanced Engineering Materials*, 19 (2017) 1700270.

945 [53] Z. Ansari, S.S. Singha, A. Saha, K. Sen, Hassle free synthesis of nanodimensional Ni, Cu and Zn
946 sulfides for spectral sensing of Hg, Cd and Pb: A comparative study, *Spectrochimica Acta Part A: Molecular*
947 *and Biomolecular Spectroscopy*, 176 (2017) 67-78.

948 [54] J. Li, Q. Wang, Z. Guo, H. Ma, Y. Zhang, B. Wang, D. Bin, Q. Wei, Highly selective fluorescent
949 chemosensor for detection of Fe^{3+} based on $\text{Fe}_3\text{O}_4@ZnO$, *Scientific Reports*, 6 (2016) 1-8.

950 [55] A. Shahat, M.R. Awual, M. Naushad, Functional ligand anchored nanomaterial based facial adsorbent
951 for cobalt (II) detection and removal from water samples, *Chemical Engineering Journal*, 271 (2015) 155-
952 163.

953 [56] M.R. Awual, M.M. Hasan, G.E. Eldesoky, M.A. Khaleque, M.M. Rahman, M. Naushad, Facile
954 mercury detection and removal from aqueous media involving ligand impregnated conjugate nanomaterials,
955 *Chemical Engineering Journal*, 290 (2016) 243-251.

956 [57] Y. Cao, W. Wu, S. Wang, H. Peng, X. Hu, Y. Yu, Monolayer gC_3N_4 fluorescent sensor for sensitive
957 and selective colorimetric detection of silver ion from aqueous samples, *Journal of Fluorescence*, 26 (2016)
958 739-744.

959 [58] A. Kaur, G. Kaur, A. Singh, N. Singh, N. Kaur, Polyamine based ratiometric fluorescent chemosensor
960 for strontium metal ion in aqueous medium: application in tap water, river water, and in oral care, *ACS*
961 *Sustainable Chemistry & Engineering*, 4 (2016) 94-101.

962 [59] H.-R. Fu, Y. Zhao, T. Xie, M.-L. Han, L.-F. Ma, S.-Q. Zang, Stable dye-encapsulated indium–organic
963 framework as dual-emitting sensor for the detection of $\text{Hg}^{2+}/\text{Cr}_2\text{O}_7^{2-}$ and a wide range of nitro-compounds,
964 *Journal of Materials Chemistry C*, 6 (2018) 6440-6448.

965 [60] X.-Y. Xu, B. Yan, Fabrication and application of a ratiometric and colorimetric fluorescent probe for
966 Hg²⁺ based on dual-emissive metal–organic framework hybrids with carbon dots and Eu³⁺, *Journal of*
967 *Materials Chemistry C*, 4 (2016) 1543-1549.

968 [61] P. Samanta, A.V. Desai, S. Sharma, P. Chandra, S.K. Ghosh, Selective recognition of Hg²⁺ ion in water
969 by a functionalized metal–Organic framework (MOF) based chemodosimeter, *Inorganic Chemistry*, 57
970 (2018) 2360-2364.

971 [62] S.A.A. Razavi, M.Y. Masoomi, A. Morsali, Double solvent sensing method for improving sensitivity
972 and accuracy of Hg (II) detection based on different signal transduction of a tetrazine-functionalized
973 pillared metal–organic framework, *Inorganic Chemistry*, 56 (2017) 9646-9652.

974 [63] A. Pankajakshan, D. Kuznetsov, S. Mandal, Ultrasensitive detection of Hg (II) ions in aqueous medium
975 using zinc-based metal–organic framework, *Inorganic Chemistry*, 58 (2019) 1377-1381.

976 [64] P. Wu, Y. Liu, Y. Liu, J. Wang, Y. Li, W. Liu, J. Wang, Cadmium-based metal–organic framework as
977 a highly selective and sensitive ratiometric luminescent sensor for mercury (II), *Inorganic Chemistry*, 54
978 (2015) 11046-11048.

979 [65] Z. Xiaoxiong, Z. Wenjun, L. Cuiliu, Q. Xiaohong, Z. Chengyu, Eu³⁺ postdoped UiO-66-type metal–
980 organic framework as a luminescent sensor for Hg²⁺ detection in aqueous media, *Inorganic Chemistry*, 58
981 (2019) 3910-3915.

982 [66] H. Tan, B. Liu, Y. Chen, Lanthanide coordination polymer nanoparticles for sensing of mercury (II)
983 by photoinduced electron transfer, *ACS Nano*, 6 (2012) 10505-10511.

984 [67] Z.-J. Wang, L.-J. Han, X.-J. Gao, H.-G. Zheng, Three Cd (II) MOFs with different functional groups:
985 selective CO₂ capture and metal ions detection, *Inorganic Chemistry*, 57 (2018) 5232-5239.

986 [68] A. Shahat, H.M. Hassan, H.M. Azzazy, Optical metal-organic framework sensor for selective
987 discrimination of some toxic metal ions in water, *Analytica Chimica Acta*, 793 (2013) 90-98.

988 [69] S. Govindaraju, P. Puthiaraj, M.-H. Lee, K. Yun, Photoluminescent AuNCs@UiO-66 for ultrasensitive
989 detection of mercury in water samples, *ACS Omega*, 3 (2018) 12052-12059.

990 [70] H. Zhai, Y. Bai, J. Qin, F. Feng, Colorimetric and ratiometric fluorescence dual-mode sensing of
991 glucose based on carbon quantum dots and potential UV/fluorescence of o-diaminobenzene, *Sensors*, 19
992 (2019) 674.

993 [71] D.K. Singha, P. Mahata, Highly selective and sensitive luminescence turn-on-based sensing of Al³⁺
994 ions in aqueous medium using a MOF with free functional sites, *Inorganic Chemistry*, 54 (2015) 6373-
995 6379.

996 [72] W.-X. Li, J.-H. Gu, H.-X. Li, M. Dai, D.J. Young, H.-Y. Li, J.-P. Lang, Post-synthetic modification of
997 a two-dimensional metal–organic framework via photodimerization enables highly selective luminescent
998 sensing of aluminum (III), *Inorganic Chemistry*, 57 (2018) 13453-13460.

999 [73] T. Rasheed, F. Nabeel, Luminescent metal-organic frameworks as potential sensory materials for
1000 various environmental toxic agents, *Coordination Chemistry Reviews*, 401 (2019) 213065.

1001 [74] T. Rasheed, F. Nabeel, M. Adeel, M. Bilal, H.M. Iqbal, “Turn-on” fluorescent sensor-based probing
1002 of toxic Hg(II) and Cu(II) with potential intracellular monitoring, *Biocatalysis and Agricultural*
1003 *Biotechnology*, 17 (2019) 696-701.

1004 [75] Y. Gao, X. Zhang, W. Sun, Z. Liu, A robust microporous metal–organic framework as a highly
1005 selective and sensitive, instantaneous and colorimetric sensor for Eu³⁺ ions, *Dalton Transactions*, 44 (2015)
1006 1845-1849.

1007 [76] F.Y. Yi, J.P. Li, D. Wu, Z.M. Sun, A series of multifunctional metal–organic frameworks showing
1008 excellent luminescent sensing, sensitization, and adsorbent abilities, *Chemistry–A European Journal*, 21
1009 (2015) 11475-11482.

1010 [77] J. An, C.M. Shade, D.A. Chengelis-Czegan, S. Petoud, N.L. Rosi, Zinc-adeninate metal– organic
1011 framework for aqueous encapsulation and sensitization of near-infrared and visible emitting lanthanide
1012 cations, *Journal of the American Chemical Society*, 133 (2011) 1220-1223.

1013 [78] W. Gong, P. Das, S. Samanta, J. Xiong, W. Pan, Z. Gu, J. Zhang, J. Qu, Z. Yang, Redefining the photo-
1014 stability of common fluorophores with triplet state quenchers: mechanistic insights and recent updates,
1015 *Chemical Communications*, 55 (2019) 8695-8704.

1016 [79] X. Luo, Y. Han, X. Chen, W. Tang, T. Yue, Z. Li, Carbon dots derived fluorescent nanosensors as
1017 versatile tools for food quality and safety assessment: A review, *Trends in Food Science & Technology*, 95
1018 (2020) 149-161.

1019 [80] N. Bhardwaj, S.K. Bhardwaj, M.K. Nayak, J. Mehta, K.-H. Kim, A. Deep, Fluorescent nanobiosensors
1020 for the targeted detection of foodborne bacteria, *TrAC Trends in Analytical Chemistry*, 97 (2017) 120-135.

1021 [81] J. Shi, F. Tian, J. Lyu, M. Yang, Nanoparticle based fluorescence resonance energy transfer (FRET)
1022 for biosensing applications, *Journal of Materials Chemistry B*, 3 (2015) 6989-7005.

1023 [82] B. Gu, Q. Zhang, Recent advances on functionalized upconversion nanoparticles for detection of small
1024 molecules and ions in biosystems, *Advanced Science*, 5 (2018) 1700609.

1025 [83] J. Zhang, F. Cheng, J. Li, J.-J. Zhu, Y. Lu, Fluorescent nanoprobe for sensing and imaging of metal
1026 ions: Recent advances and future perspectives, *Nano Today*, 11 (2016) 309-329.

1027 [84] L. Ou, X. Li, H. Liu, L. Li, X. Chu, Poly (thymine)-templated fluorescent copper nanoparticles for
1028 ultrasensitive label-free detection of lead ion, *Analytical Sciences*, 30 (2014) 723-727.

1029 [85] J. Chen, J. Liu, Z. Fang, L. Zeng, Random dsDNA-templated formation of copper nanoparticles as
1030 novel fluorescence probes for label-free lead ions detection, *Chemical Communications*, 48 (2012) 1057-
1031 1059.

1032 [86] L.E. Silva-De Hoyos, V. Sánchez-Mendieta, A.R. Vilchis-Nestor, M.A. Camacho-López, Biogenic
1033 silver nanoparticles as sensors of Cu²⁺ and Pb²⁺ in aqueous solutions, *Universal Journal of Materials
1034 Science*, 5 (2017) 29-37.

1035 [87] Y.-S. Wu, F.-F. Huang, Y.-W. Lin, Fluorescent detection of lead in environmental water and urine
1036 samples using enzyme mimics of catechin-synthesized Au nanoparticles, *ACS Applied Materials &
1037 Interfaces*, 5 (2013) 1503-1509.

1038 [88] S. Wang, J. Sun, F. Gao, A turn-on near-infrared fluorescent chemosensor for selective detection of
1039 lead ions based on a fluorophore-gold nanoparticle assembly, *Analyst*, 140 (2015) 4001-4006.

1040 [89] C.J. Breshike, R.A. Riskowski, G.F. Strouse, Leaving forster resonance energy transfer behind:
1041 nanometal surface energy transfer predicts the size-enhanced energy coupling between a metal nanoparticle
1042 and an emitting dipole, *The Journal of Physical Chemistry C*, 117 (2013) 23942-23949.

1043 [90] L. Chun, C.-Z. HUANG, Detection of lead ions in water based on the surface energy transfer between
1044 gold nanoparticles and fluorescent dyes, *Chinese Journal of Analytical Chemistry*, 42 (2014) 1195-1198.

1045 [91] C.H. Chung, J.H. Kim, J. Jung, B.H. Chung, Nuclease-resistant DNA aptamer on gold nanoparticles
1046 for the simultaneous detection of Pb²⁺ and Hg²⁺ in human serum, *Biosensors and Bioelectronics*, 41 (2013)
1047 827-832.

1048 [92] G. Chen, H. Qiu, P.N. Prasad, X. Chen, Upconversion nanoparticles: design, nanochemistry, and
1049 applications in theranostics, *Chemical Reviews*, 114 (2014) 5161-5214.

1050 [93] Y. Zhang, L. Wu, Y. Tang, Y. Su, Y. Lv, An upconversion fluorescence based turn-on probe for
1051 detecting lead (II) ions, *Analytical Methods*, 6 (2014) 9073-9077.

1052 [94] S. Wu, N. Duan, Z. Shi, C. Fang, Z. Wang, Dual fluorescence resonance energy transfer assay between
1053 tunable upconversion nanoparticles and controlled gold nanoparticles for the simultaneous detection of Pb²⁺
1054 and Hg²⁺, *Talanta*, 128 (2014) 327-336.

1055 [95] S. Xu, S. Xu, Y. Zhu, W. Xu, P. Zhou, C. Zhou, B. Dong, H. Song, A novel upconversion, fluorescence
1056 resonance energy transfer biosensor (FRET) for sensitive detection of lead ions in human serum, *Nanoscale*,
1057 6 (2014) 12573-12579.

1058 [96] L. Gong, H. Kuai, S. Ren, X.-H. Zhao, S.-Y. Huan, X.-B. Zhang, W. Tan, Ag nanocluster-based label-
1059 free catalytic and molecular beacons for amplified biosensing, *Chemical Communications*, 51 (2015)
1060 12095-12098.

1061 [97] M. Liu, F. Tang, Z. Yang, J. Xu, X. Yang, Recent progress on gold-nanocluster-based fluorescent
1062 probe for environmental analysis and biological sensing, *Journal of Analytical Methods in Chemistry*, 2019
1063 (2019) <https://doi.org/10.1155/2019/1095148>.

1064 [98] C. Song, J. Xu, Y. Chen, L. Zhang, Y. Lu, Z. Qing, DNA-templated fluorescent nanoclusters for metal
1065 ions detection, *Molecules*, 24 (2019) 4189.

1066 [99] Y. Yang, A. Han, R. Li, G. Fang, J. Liu, S. Wang, Synthesis of highly fluorescent gold nanoclusters
1067 and their use in sensitive analysis of metal ions, *Analyst*, 142 (2017) 4486-4493.

1068 [100] Z. Yuan, M. Peng, Y. He, E.S. Yeung, Functionalized fluorescent gold nanodots: synthesis and
1069 application for Pb²⁺ sensing, *Chemical Communications*, 47 (2011) 11981-11983.

1070 [101] H. Zhu, T. Yu, H. Xu, K. Zhang, H. Jiang, Z. Zhang, Z. Wang, S. Wang, Fluorescent nanohybrid of
1071 gold nanoclusters and quantum dots for visual determination of lead ions, *ACS Applied Materials &
1072 Interfaces*, 6 (2014) 21461-21467.

1073 [102] C. Wang, J. Wu, K. Jiang, M.G. Humphrey, C. Zhang, Stable Ag nanoclusters-based nano-sensors:
1074 rapid sonochemical synthesis and detecting Pb²⁺ in living cells, *Sensors and Actuators B: Chemical*, 238
1075 (2017) 1136-1143.

1076 [103] B. Zhang, C. Wei, Highly sensitive and selective detection of Pb²⁺ using a turn-on fluorescent aptamer
1077 DNA silver nanoclusters sensor, *Talanta*, 182 (2018) 125-130.

1078 [104] C. Li, G. Shi, Carbon nanotube-based fluorescence sensors, *Journal of Photochemistry and
1079 Photobiology C: Photochemistry Reviews*, 19 (2014) 20-34.

1080 [105] S.E. Wang, S. Si, Aptamer biosensing platform based on carbon nanotube long-range energy transfer
1081 for sensitive, selective and multicolor fluorescent heavy metal ion analysis, *Analytical Methods*, 5 (2013)
1082 2947-2953.

1083 [106] S.M. Taghdisi, S.S. Emrani, K. Tabrizian, M. Ramezani, K. Abnous, A.S. Emrani, Ultrasensitive
1084 detection of lead (II) based on fluorescent aptamer-functionalized carbon nanotubes, *Environmental
1085 Toxicology and Pharmacology*, 37 (2014) 1236-1242.

1086 [107] Y. Huang, N. He, Q. Kang, D. Shen, X. Wang, Y. Wang, L. Chen, A carbon dot-based fluorescent
1087 nanoprobe for the associated detection of iron ions and the determination of the fluctuation of ascorbic acid
1088 induced by hypoxia in cells and in vivo, *Analyst*, 144 (2019) 6609-6616.

1089 [108] P. Devi, P. Rajput, A. Thakur, K.-H. Kim, P. Kumar, Recent advances in carbon quantum dot-based
1090 sensing of heavy metals in water, *TrAC Trends in Analytical Chemistry*, 114 (2019) 171-195.

1091 [109] D. Yoo, Y. Park, B. Cheon, M.-H. Park, Carbon dots as an effective fluorescent sensing platform for
1092 metal ion detection, *Nanoscale Research Letters*, 14 (2019) 1-13.

1093 [110] X. Wang, P. Yang, Q. Feng, T. Meng, J. Wei, C. Xu, J. Han, Green preparation of fluorescent carbon
1094 quantum dots from cyanobacteria for biological imaging, *Polymers*, 11 (2019) 616.

1095 [111] Y. Liu, Q. Zhou, J. Li, M. Lei, X. Yan, Selective and sensitive chemosensor for lead ions using
1096 fluorescent carbon dots prepared from chocolate by one-step hydrothermal method, *Sensors and Actuators
1097 B: Chemical*, 237 (2016) 597-604.

1098 [112] A. Kumar, A.R. Chowdhuri, D. Laha, T.K. Mahto, P. Karmakar, S.K. Sahu, Green synthesis of carbon
1099 dots from *Ocimum sanctum* for effective fluorescent sensing of Pb²⁺ ions and live cell imaging, *Sensors and
1100 Actuators B: Chemical*, 242 (2017) 679-686.

1101 [113] R. Bandi, R. Dadigala, B.R. Gangapuram, V. Guttena, Green synthesis of highly fluorescent nitrogen-
1102 doped carbon dots from *Lantana camara* berries for effective detection of lead (II) and bioimaging, *Journal
1103 of Photochemistry and Photobiology B: Biology*, 178 (2018) 330-338.

1104 [114] J. Xu, X. Jie, F. Xie, H. Yang, W. Wei, Z. Xia, Flavonoid moiety-incorporated carbon dots for
1105 ultrasensitive and highly selective fluorescence detection and removal of Pb²⁺, *Nano Research*, 11 (2018)
1106 3648-3657.

1107 [115] A. Gupta, N.C. Verma, S. Khan, S. Tiwari, A. Chaudhary, C.K. Nandi, Paper strip based and live cell
1108 ultrasensitive lead sensor using carbon dots synthesized from biological media, *Sensors and Actuators B:
1109 Chemical*, 232 (2016) 107-114.

1110 [116] J. Yang, J.-X. Wu, Q.-F. Lü, T.-T. Lin, Facile preparation of lignosulfonate-graphene oxide-
1111 polyaniline ternary nanocomposite as an effective adsorbent for Pb (II) ions, *ACS Sustainable Chemistry
1112 & Engineering*, 2 (2014) 1203-1211.

1113 [117] Y. Jiang, Y. Wang, F. Meng, B. Wang, Y. Cheng, C. Zhu, N-doped carbon dots synthesized by rapid
1114 microwave irradiation as highly fluorescent probes for Pb²⁺ detection, *New Journal of Chemistry*, 39 (2015)
1115 3357-3360.

1116 [118] S.S. Wee, Y.H. Ng, S.M. Ng, Synthesis of fluorescent carbon dots via simple acid hydrolysis of
1117 bovine serum albumin and its potential as sensitive sensing probe for lead (II) ions, *Talanta*, 116 (2013) 71-
1118 76.

1119 [119] Q. Wang, S. Zhang, H. Ge, G. Tian, N. Cao, Y. Li, A fluorescent turn-off/on method based on carbon
1120 dots as fluorescent probes for the sensitive determination of Pb²⁺ and pyrophosphate in an aqueous solution,
1121 *Sensors and Actuators B: Chemical*, 207 (2015) 25-33.

1122 [120] Y. Liu, Q. Zhou, Y. Yuan, Y. Wu, Hydrothermal synthesis of fluorescent carbon dots from sodium
1123 citrate and polyacrylamide and their highly selective detection of lead and pyrophosphate, *Carbon*, 115
1124 (2017) 550-560.

1125 [121] Z.-X. Wang, X.-H. Yu, F. Li, F.-Y. Kong, W.-X. Lv, D.-H. Fan, W. Wang, Preparation of boron-
1126 doped carbon dots for fluorometric determination of Pb (II), Cu (II) and pyrophosphate ions, *Microchimica*
1127 *Acta*, 184 (2017) 4775-4783.

1128 [122] Y. Tian, A. Kelarakis, L. Li, F. Zhao, Y. Wang, W. Wang, Q. Yang, Z. Ye, X. Guo, Facile
1129 fluorescence “turn on” sensing of lead ions in water via carbon nanodots immobilized in spherical
1130 polyelectrolyte brushes, *Frontiers in Chemistry*, 6 (2018) 470.

1131 [123] F. Yarur, J.-R. Macairan, R. Naccache, Ratiometric detection of heavy metal ions using fluorescent
1132 carbon dots, *Environmental Science: Nano*, 6 (2019) 1121-1130.

1133 [124] L. Wang, H.-X. Cao, Y.-S. He, C.-G. Pan, T.-K. Sun, X.-Y. Zhang, C.-Y. Wang, G.-X. Liang, Facile
1134 preparation of amino-carbon dots/gold nanoclusters FRET ratiometric fluorescent probe for sensing of
1135 Pb²⁺/Cu²⁺, *Sensors and Actuators B: Chemical*, 282 (2019) 78-84.

1136 [125] W. Liu, X. Wang, Y. Wang, J. Li, D. Shen, Q. Kang, L. Chen, Ratiometric fluorescence sensor based
1137 on dithiothreitol modified carbon dots-gold nanoclusters for the sensitive detection of mercury ions in water
1138 samples, *Sensors and Actuators B: Chemical*, 262 (2018) 810-817.

1139 [126] X. Chen, N. Zhai, J.H. Snyder, Q. Chen, P. Liu, L. Jin, Q. Zheng, F. Lin, J. Hu, H. Zhou, Colorimetric
1140 detection of Hg²⁺ and Pb²⁺ based on peroxidase-like activity of graphene oxide-gold nanohybrids,
1141 *Analytical Methods*, 7 (2015) 1951-1957.

1142 [127] S. Zhang, D. Zhang, X. Zhang, D. Shang, Z. Xue, D. Shan, X. Lu, Ultratrace naked-eye colorimetric
1143 detection of Hg²⁺ in wastewater and serum utilizing mercury-stimulated peroxidase mimetic activity of
1144 reduced graphene oxide-PEI-Pd nanohybrids, *Analytical Chemistry*, 89 (2017) 3538-3544.

1145 [128] L. Zhi, W. Zuo, F. Chen, B. Wang, 3D MoS₂ composition aerogels as chemosensors and adsorbents
1146 for colorimetric detection and high-capacity adsorption of Hg²⁺, *ACS Sustainable Chemistry &*
1147 *Engineering*, 4 (2016) 3398-3408.

1148 [129] Z. Yan, H. Xue, K. Berning, Y.-W. Lam, C.-S. Lee, Identification of multifunctional graphene-gold
1149 nanocomposite for environment-friendly enriching, separating, and detecting Hg²⁺ simultaneously, *ACS*
1150 *Applied Materials & Interfaces*, 6 (2014) 22761-22768.

1151 [130] Y. Liu, X. Wang, H. Wu, Reusable DNA-functionalized-graphene for ultrasensitive mercury (II)
1152 detection and removal, *Biosensors and Bioelectronics*, 87 (2017) 129-135.

1153 [131] W. Xiaofei, L. Ruiyi, L. Zaijun, L. Junkang, W. Guangli, G. Zhiguo, Synthesis of double gold
1154 nanoclusters/graphene oxide and its application as a new fluorescence probe for Hg²⁺ detection with greatly
1155 enhanced sensitivity and rapidity, *RSC Advances*, 4 (2014) 24978-24985.

1156 [132] X. Yu, W. Liu, X. Deng, S. Yan, Z. Su, Gold nanocluster embedded bovine serum albumin
1157 nanofibers-graphene hybrid membranes for the efficient detection and separation of mercury ion, *Chemical*
1158 *Engineering Journal*, 335 (2018) 176-184.

1159 [133] Y. Liu, M. Deng, X. Tang, T. Zhu, Z. Zang, X. Zeng, S. Han, Luminescent AIZS-GO nanocomposites
1160 as fluorescent probe for detecting copper (II) ion, *Sensors and Actuators B: Chemical*, 233 (2016) 25-30.

1161 [134] L. Kong, J. Wang, G. Zheng, J. Liu, A highly sensitive protocol (FRET/SIMNSEF) for the
1162 determination of mercury ions: a unity of fluorescence quenching of graphene and enhancement of
1163 nanogold, *Chemical Communications*, 47 (2011) 10389-10391.

1164 [135] J. Huang, X. Gao, J. Jia, J.-K. Kim, Z. Li, Graphene oxide-based amplified fluorescent biosensor for
1165 Hg²⁺ detection through hybridization chain reactions, *Analytical Chemistry*, 86 (2014) 3209-3215.

1166 [136] J.R. Zhang, W.T. Huang, W.Y. Xie, T. Wen, H.Q. Luo, N.B. Li, Highly sensitive, selective, and rapid
1167 fluorescence Hg^{2+} sensor based on DNA duplexes of poly (dT) and graphene oxide, *Analyst*, 137 (2012)
1168 3300-3305.

1169 [137] K. Zhai, Y. Liu, D. Xiang, G. Guo, T. Wan, H. Hu, Dual color fluorescence quantitative detection of
1170 mercury in soil with graphene oxide and dye-labeled nucleic acids, *Analytical Methods*, 7 (2015) 3827-
1171 3832.

1172 [138] S. Pang, S. Liu, X. Su, An ultrasensitive sensing strategy for the detection of lead (II) ions based on
1173 the intermolecular G-quadruplex and graphene oxide, *Sensors and Actuators B: Chemical*, 208 (2015) 415-
1174 420.

1175 [139] X. Cui, L. Zhu, J. Wu, Y. Hou, P. Wang, Z. Wang, M. Yang, A fluorescent biosensor based on carbon
1176 dots-labeled oligodeoxyribonucleotide and graphene oxide for mercury (II) detection, *Biosensors and*
1177 *Bioelectronics*, 63 (2015) 506-512.

1178 [140] Z.S. Qian, X.Y. Shan, L.J. Chai, J.R. Chen, H. Feng, A fluorescent nanosensor based on graphene
1179 quantum dots-aptamer probe and graphene oxide platform for detection of lead (II) ion, *Biosensors and*
1180 *Bioelectronics*, 68 (2015) 225-231.

1181 [141] X. Sun, Y. Peng, Y. Lin, L. Cai, F. Li, B. Liu, G-quadruplex formation enhancing energy transfer in
1182 self-assembled multilayers and fluorescence recognize for Pb^{2+} ions, *Sensors and Actuators B: Chemical*,
1183 255 (2018) 2121-2125.

1184 [142] M. Liu, H. Zhao, S. Chen, H. Yu, Y. Zhang, X. Quan, A “turn-on” fluorescent copper biosensor based
1185 on DNA cleavage-dependent graphene-quenched DNAzyme, *Biosensors and Bioelectronics*, 26 (2011)
1186 4111-4116.

1187 [143] M. Liu, H. Zhao, S. Chen, H. Yu, Y. Zhang, X. Quan, Label-free fluorescent detection of Cu (II) ions
1188 based on DNA cleavage-dependent graphene-quenched DNAzymes, *Chemical Communications*, 47 (2011)
1189 7749-7751.

1190 [144] X.-H. Zhao, R.-M. Kong, X.-B. Zhang, H.-M. Meng, W.-N. Liu, W. Tan, G.-L. Shen, R.-Q. Yu,
1191 Graphene-DNAzyme based biosensor for amplified fluorescence “turn-on” detection of Pb^{2+} with a high
1192 selectivity, *Analytical Chemistry*, 83 (2011) 5062-5066.

1193 [145] Y. Wen, C. Peng, D. Li, L. Zhuo, S. He, L. Wang, Q. Huang, Q.-H. Xu, C. Fan, Metal ion-modulated
1194 graphene-DNAzyme interactions: design of a nanoprobe for fluorescent detection of lead (II) ions with high
1195 sensitivity, selectivity and tunable dynamic range, *Chemical Communications*, 47 (2011) 6278-6280.

1196 [146] J. Huang, Q. Zheng, J.-K. Kim, Z. Li, A molecular beacon and graphene oxide-based fluorescent
1197 biosensor for Cu^{2+} detection, *Biosensors and Bioelectronics*, 43 (2013) 379-383.

1198 [147] D. Dinda, B.K. Shaw, S.K. Saha, Thymine functionalized graphene oxide for fluorescence “turn-off-
1199 on” sensing of Hg^{2+} and I^- in aqueous medium, *ACS Applied Materials & Interfaces*, 7 (2015) 14743-14749.

1200 [148] X. Fu, T. Lou, Z. Chen, M. Lin, W. Feng, L. Chen, “Turn-on” fluorescence detection of lead ions
1201 based on accelerated leaching of gold nanoparticles on the surface of graphene, *ACS Applied Materials &*
1202 *Interfaces*, 4 (2012) 1080-1086.

1203 [149] M. Li, X. Zhou, W. Ding, S. Guo, N. Wu, Fluorescent aptamer-functionalized graphene oxide
1204 biosensor for label-free detection of mercury (II), *Biosensors and Bioelectronics*, 41 (2013) 889-893.

1205 [150] B. Wang, J. Hai, Z. Liu, Q. Wang, Z. Yang, S. Sun, Selective detection of iron (III) by rhodamine-
1206 modified Fe_3O_4 nanoparticles, *Angewandte Chemie International Edition*, 49 (2010) 4576-4579.

1207 [151] M. Li, S.K. Cushing, H. Liang, S. Suri, D. Ma, N. Wu, Plasmonic nanorice antenna on triangle
1208 nanoarray for surface-enhanced Raman scattering detection of hepatitis B virus DNA, *Analytical*
1209 *Chemistry*, 85 (2013) 2072-2078.

1210 [152] Y. Hu, F. Zhao, S. Hu, Y. Dong, D. Li, Z. Su, A novel turn-on colorimetric and fluorescent sensor
1211 for Fe^{3+} and its application in living cells, *Journal of Photochemistry and Photobiology A: Chemistry*, 332
1212 (2017) 351-356.

1213
1214
1215